The Rainfall and Erosivity Database for Mexico (1968-2017)

Viviana Marcela Varón-Ramírez[1,2], Douglas A. Gómez-Latorre[3], Carlos Eduardo Arroyo-Cruz[1,2], Alberto Gómez-Tagle[4], Blanca Lucía Prado Pano[5], Ronald R. Gutierrez[6], Deyanira Lobo-Luján[7], and Mario Guevara[1]

[1]Instituto de Geociencias, Universidad Nacional Autónoma de México, Campus UNAM Juriquilla, Blvd Juriquilla 3001, Juriquilla, Querétaro, CP 76230, México
[2]Posgrado en Ciencias de la Tierra, Instituto de Geociencias, Universidad Nacional Autónoma de México, Campus UNAM Juriquilla, Blvd Juriquilla 3001, Juriquilla, Querétaro, CP 76230, México.
[3]Corporación Colombiana de Investigación Agropecuaria - AGROSAVIA, Centro de Investigación Tibaitatá, Mosquera-Cundinamarca, Colombia
[4]Instituto de Investigaciones sobre los Recursos Naturales - INIRENA, Universidad Michoacana de San Nicolás de Hidalgo. Morelia, Mexico
[5]Instituto de Geología - Universidad Nacional Autónoma de México. Campus UNAM Ciudad Universitaria. Ciudad de Mexico. Mexico.
[6]Centro de Investigación y Tecnología del Agua (CITA), Universidad de Ingeniería y Tecnología (UTEC), Lima, Perú
[7]Instituto de Edafología - Universidad Central de Venezuela. Maracay, Aragua. Venezuela

Correspondence: Viviana Marcela Varón-Ramírez (viviana.varon@geociencias.unam.mx) and Mario Guevara (mguevara@geociencias.unam.mx)

Abstract. Soil water erosion is the dominant soil degradation driver worldwide. Rainfall erosivity (also known as the R factor) quantifies the potential of rainfall to cause soil water erosion and is regarded as a dominant factor determining it. This contribution presents the first annual R factor database across the continental Mexico for three climate normals (1968–1997, 1978–2007, and 1988–2017). The workflow comprised three main steps. Firstly, a harmonaized daily rainfall time series dataset was obtained by compiling and harmonizing (through quality control, homogeneity analysis and gap-filling) 5,410 raw rainfall time series distributed across Mexico. Secondly, three combinations of the α and β coefficients in a power model were tested to estimate daily R factors using three validation databases at global, national, and local scales. Thirdly, a validated and continuously distributed annual R factor for all three climate normal was obtained. Thus, the database presented herein encompasses 1,369 (climate normal 1968–1997) , 1,678 (climate normal 1978–2007), and 1,676 (climate normal 1988–2017) rainfall time series and the corresponding R factor. Our results indicate that the median values of the R factor for the three climate normals were 3,245; 3,070; and 3,327 MJ mm ha^{-1} h^{-1} yr^{-1}, respectively. The statistical distribution of the R factor is right-skewed for the three climate normals, with high erosivity values reaching >12000 MJ mm ha^{-1} h^{-1} yr^{-1} in all cases. The R factor across Mexico showed a strong ecoregional differentiation, with the highest values concentrated in the Tropical Rain Forest and Tropical Dry Forest ecoregions, whereas the North American Deserts and Mediterranean California exhibited the lowest values. The annual behavior of the R factor was similar for the three climate normals. However, September had the highest contribution to the annual R factor. By identifying areas with higher susceptibility to soil loss due to rainfall action and providing spatially distributed and well-documented estimates, we believe that the present R factor database has the potential to support the study of soil water erosion in the continental Mexico at country scale. Said database is available from

a scholarly-accepted repository at https://doi.org/10.6073/pasta/dd2b30e28ee25ff2d60d8a9f436951d2 (Varón-Ramírez et al., 2026) for public consultation.

Keywords: legacy climate data, climate normals, daily rainfall erosivity, R factor, climatol package.

1 Introduction

Soil water erosion (SWE) refers to the soil displacement from its original location due to water action, such as rainfall, overland flow, and irrigation (Nearing, 2013). SWE represents the dominant soil degradation issue at the global scale because it affects nearly 33% of the World's surface (Pennock, 2019). SWE has both on-site and off-site effects. On-site, soil loses its natural capacity to store water, nutrients, and organic carbon (Hatfield et al., 2017), affecting, for instance, food security. Off-site, the eroded soil triggers environmental issues such as water pollution, dam siltation, eutrophication of water bodies, contamination of coastal and marine ecosystems, and overall environmental damage (Feng et al., 2023; Borrelli et al., 2022; Guo et al., 2020). These widespread impacts underscore the urgent need to study SWE at national scales to guide effective land and water management, especially in tropical countries (Rosas and Gutierrez, 2020; Varón-Ramírez and Guevara, 2024).

Rainfall erosivity is the potential of rainfall to cause SWE (Nearing et al., 2017). Research evidence shows that rainfall erosivity is the dominant factor influencing SWE. As extreme rainfall events are expected to increase in frequency and intensity in tropical zones, rainfall erosivity is also expected to rise (Borrelli et al., 2020). Mexico is exhibiting this pattern as the temporal distribution of rainfall has become more extreme, with longer droughts and increasingly severe rainfall events (Porrúa et al., 2020). Thus, understanding rainfall erosivity patterns across Mexico and analyzing them over a multi-year period is essential for enhancing soil sustainability and informed decision-making in soil conservation at national scale.

Rainfall erosivity—often represented as the R factor—captures the combined effect of raindrop impact and water flow. Wischmeier and Smith (1958) defined the rainfall erosivity of a storm as energy $\times$ times $\times$ intensity (EI). The E term refers to the total storm energy, and the I term refers to the maximum 30-min intensity $I30$. The R factor is commonly expressed as the $EI30$ index, and over multi-year period, the R factor represents the mean annual rainfall erosivity, and the yearly rainfall erosivity (R_y) results from totaling the rainfall erosivities for all storms in a year. Several studies have shown that higher-resolution data (e.g., minute-resolution) yield more accurate erosivity estimates for a specific time period (Yin et al., 2015). High-resolution rainfall data is however challenging to obtain, especially for national-scale analyses in developing countries (Rosas and Gutierrez, 2020). Consequently, a common approach in these contexts is to construct empirical relationships of erosivity based on insufficient finer-resolution rainfall data and/or long coarse-resolution rainfall data (e.g., daily, monthly, and annual).

Mexico lacks a public database of high-temporal-resolution (i.e., sub-hourly) rainfall time series. The existing data is incomplete and has breakpoints pitfalls that limit studying climatic-related processes at national scales (Cuervo-Robayo et al., 2020). Thus, SWE-related studies have computed the R factor using coarse-resolution rainfall time series (monthly or annual) for specific regions (Benites et al., 2020; González et al., 2016) and/or developed empirical relationships using daily rainfall to approximate $EI30$. The Mexican Meteorological Service provides a rainfall database (daily records from approximately 5,454 weather stations across Mexico, with time series spanning heterogeneous periods from 1900 up to 2020), which opens up the opportunity to study the national rainfall erosivity patterns.

Several models have been developed to estimate the R factor worldwide. For instance, Richardson et al. (1983) proposed a power law model by assuming that a daily rainfall could be interpreted as a single storm. This model has been used in several countries to describe rainfall erosivity patterns (Rutebuka et al., 2020). Said model nevertheless requires sufficiently long time rainfall series (e.g., at least 20 years) to capture seasonal variability and mitigate cyclical rainfall biases (Kumar et al., 2026). Therefore, access to harmonized, quality-controlled, and sufficiently long rainfall datasets is critical for users aiming to perform consistent soil erosion modeling based on the R factor and environmental assessments at regional and national scales.

The main objective of this contribution is to address the requirements for consistent and reliable model inputs to assess the impact of precipitation on SWE at national scale in Mexico. To this end, two specific objectives are defined, namely (a) to construct the first harmonized rainfall database for three climate normals (1968–1997, 1978–2007, and 1988–2017) derived from legacy climate data, and (b) to construct the first rainfall erosivity estimates across continental Mexico. Section 2 of this article elaborates on the methodological aspects of 1) development of the daily rainfall time series database, 2) identification of the best empirical relationship to estimate daily rainfall erosivity, and 3) estimation of the rainfall erosivity across Mexican territory. The results (Section 3) are then presented accordingly, and, subsequently, discussed through a critical analysis based on recent scientific literature in Section 4. We finally present our conclusions in Section 5. All the computational codes and resulting databases of this research are freely available from a scholarly-accepted repository. We believe that these products provide a basis for improving the understanding of rainfall distribution and its role in soil erosion processes across Mexico.

2 Methodology

The study area corresponds to continental Mexico (1,948,170 km^2), which is located between latitudes 14°N and 32°N and longitudes 86°W and 118°W. Mexico exhibits complex climatic features influenced by subtopical high-pressure systems over the North Atlantic and northeastern Pacific, as well as its position relative to the Intertropical Convergence Zone (de Anda Sánchez, 2020). Mexico has been clustered into seven first-level ecoregions—which represent geographical units with characteristic biodiversity (Commission for Environmental Cooperation, 1997)—, namely: Mediterranean California, North American Deserts, Semi-arid Elevations, Great Plains, Tropical Rain Forest, Tropical Dry Forest, and Temperate Sierras. Each ecoregion occupies 1.3, 28.6, 11.8, 5.5, 14.2, 16.4, and 22.3 % of the total country area, respectively (Figure 1).

This research followed a workflow of three methodological stages (Figure 2). First, we developed a rainfall time series database with daily resolution. Second, we identified the best empirical relationship to estimate erosivity using daily rainfall data. Third, we estimated the rainfall erosivity by using daily rainfall time series across the entire Mexican territory.

2.1 Data processing and quality control of rainfall time series

Developing a rainfall time series and, subsequently, a rainfall erosivity database is challenging in both spatial and temporal terms. The large diversity of topographic conditions (i.e., two principal mountain ranges and a large latitudinal extent) and

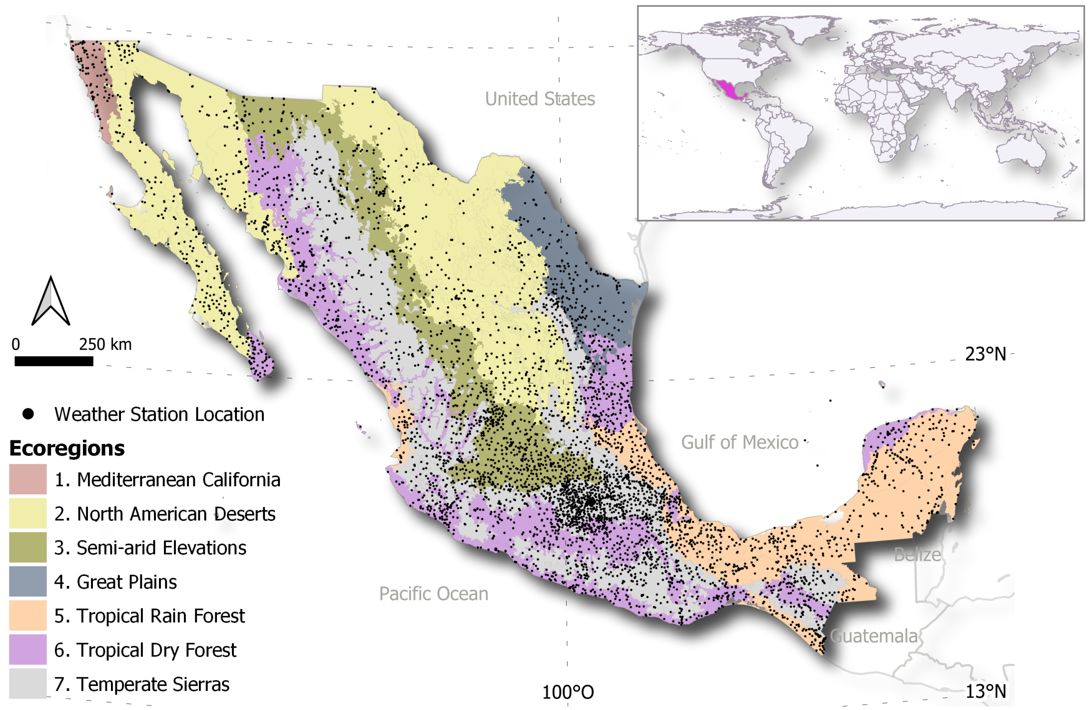

Figure 1. Ecoregions defined by the Commission for Environmental Cooperation (1997) and locations of the weather station available from the National Meteorological Service (SMN)

proximity to large water bodies from the Pacific Ocean and the Gulf of Mexico make Mexico a contrasting scenario of rainfall patterns (Carrera et al., 2024) and its hydrological-related processes(e.g., rainfall erosivity). Accurate benchmarks for understanding typical climate conditions and characterizing climate trends require a rainfall database long enough to represent its corresponding climate normal (CN), i.e., a statistical product computed over 30 years of rainfall time series (WMO, 2017). The CNs are widely used to compare recent observations, create anomaly-based datasets, and provide context for future climate projections. Considering local patterns across different CNs, these characteristics will contribute to an unprecedented rainfall time series dataset to estimate rainfall erosivity in Mexico.

On the other hand, climatology studies, such as erosivity, need a complete and reliable rainfall time series database (Yozgatligil et al., 2013). Therefore, a whole scheme of quality assurance, gap-filling, and homogenization process of the rainfall time series is needed (WMO, 2023). This quality control and homogenization process has been widely applied before rainfall erosivity analysis, in order to avoid incoherent rainfall amounts that could affect the long-term rainfall erosivity estimations (Rutebuka et al., 2020). Consequently, with a reliable rainfall database, it is possible to represent the actual rainfall characteristics in a particular region and allow soil erosion monitoring at the local and national scales in Mexico.

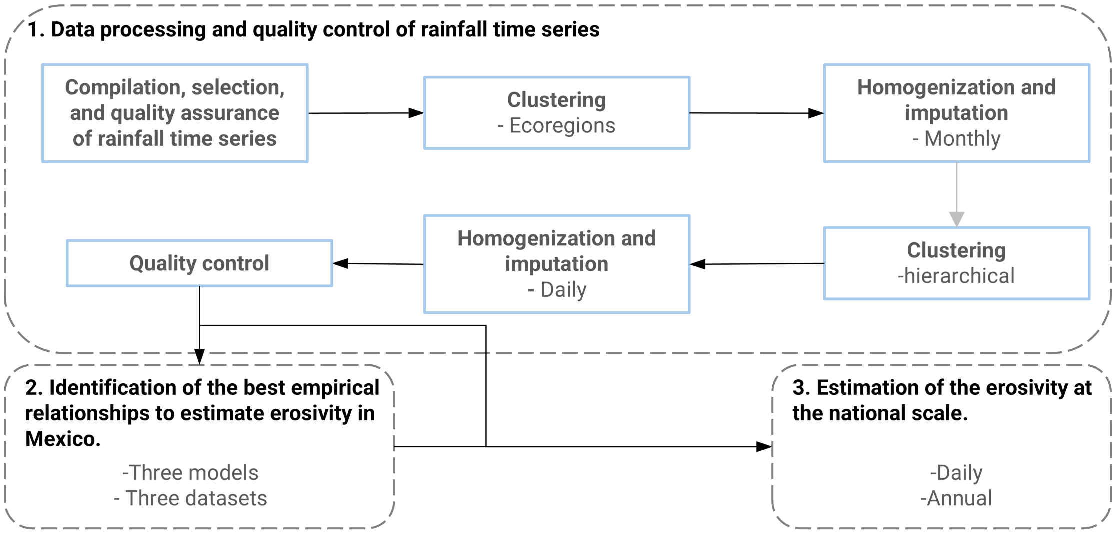

Figure 2. Workflow summarizing the three key methodological stages: (1) Development of the rainfall series database, (2) Identification of the best empirical relationships to estimate erosivity in Mexico, and (3) Estimation of the erosivity at the national scale.

The rainfall time series database was developed through four steps: first, compilation, selection, and quality assurance of the rainfall time series. Second, the clustering of the rainfall time series was based on their geographical and data attributes. Third, homogenization and data gap-filling of monthly and daily rainfall time series. Fourth, quality control of the data gap-filling process.

2.1.1 Compilation, selection, quality assurance of rainfall time series

The data were downloaded from the official National Meteorological Service website (https://smn.conagua.gob.mx/es/) in January 2022. For this project, 5,454 plain-text files were downloaded, corresponding to the daily database of the entire network of weather stations (Figure 1). After a harmonization process, 44 plain-text files without rainfall data were discarded. Finally, a set of 5,410 daily rainfall time series was obtained for use in this study.

Although the database includes records with an emission date extending to June 2020, inspection of the rainfall time series indicates that the period with the most complete and consistent data spans from 1961 to 2017. On the other hand, for erosivity estimations, it is recommended to use a historical rainfall time series of $\geq$20 years (Vantas et al., 2019; Renard and Freimund, 1994). Therefore, this study analyzed the rainfall time series in three climate normals: CN1 (1968 to 1997), CN2 (1978 to 2007), and CN3 (1988 to 2017).

Subsequently, we selected rainfall time series with less than 20% missing values (WMO, 2023), resulting in 1489, 1785, and 1728 rainfall series for CN1, CN2, and CN3, respectively (Table A1). However, long sequences of zeros and missing values

(NAs) were frequently identified within the selected rainfall series. Therefore, as part of the quality-assurance procedure, zero sequences ranging from three to six consecutive years were considered suspicious and replaced with NAs. Additionally, rainfall time series containing zero sequences longer than six years were discarded from the analysis (10, 11, and 7 series for CN1, CN2, and CN3, respectively). After applying these filters, the final dataset comprised 1479, 1774, and 1721 rainfall time series for CN1, CN2, and CN3, respectively.

2.1.2 Clustering of rainfall time series

Clustering analysis is highly recommended when gap-filling a large set of rainfall time series (Guijarro, 2014). Clustering similar rainfall time series allows us to use information from related series to fill in gaps. Rainfall patterns often exhibit spatial and temporal correlations, so data gap-filling from a group of similar series can result in more accurate estimates (Fransiska et al., 2024). In this workflow, we performed data gap-filling by clustering rainfall time series according to (1) ecoregions and (2) data dissimilarity across different environments (Figure 2). The first clustering was performed using the ecoregions of North America (Commission for Environmental Cooperation, 1997; INEGI-CONABIO-INE, 2008). The second clustering was applied after gap-filling and homogenization of the monthly series within each ecoregion, using a hierarchical cluster analysis to group time series with similar seasonality and rainfall volume patterns (Gómez-Latorre et al., 2022). The number of clusters (k) ranged from 2 to $sqrt(n)$, where n is the total number of stations in the dataset (Rohlf, 1974). The better k values for each ecoregion were found using the Hartigan cluster validation index (Hartigan, 1975). This index was identified by Todeschini et al. (2024) to perform better when evaluating 68 cluster validation indexes over 21 different datasets. However, we did not perform a clustering analysis for Mediterranean California and Great Plains ecoregions due to the small size of the ecoregions and, therefore, the amount of the rainfall time series available for those ecoregions.

2.1.3 Homogenization, data gap-filling and quality control of the rainfall time series

We followed three steps to get a complete rainfall time series for each CN: quality assurance, homogeneity analysis, and data gap-filling (WMO, 2020). In this step, quality assurance involved verifying the physical and statistical consistency of the series, discarding outliers whose standardized anomaly was outside a predefined threshold and was unrelated to any climate variability events. Outliers were removed and replaced with NA values to be filled during the data gap-filling process.

Homogeneity analysis removes the biases caused by some artificial breaks in the rainfall time series (Yan et al., 2014). These breaks result from common issues such as reading or measurement errors, instrumental changes, or atypical situations at the weather station location Guijarro (2014). We used the standard normal homogeneity test (Alexandersson, 1986) to analyse homogeneity.

To fill in missing data, we used the proportions method. This method estimates the missing information based on neighboring stations, considering the distance between each station (Paulhus and Kohler, 1952). The procedure used the three precipitation series with the highest correlation coefficient to the series that will be filled, with the condition of having been previously normalized. Then, we estimated $N_1 = \frac{A_1}{3}(\frac{N_a}{A_a} + \frac{N_b}{A_b} + \frac{N_c}{A_c})$; where N_a, N_b and N_c are the precipitation data for each of the stations with the highest correlation, while A_a, A_b and N_c are their corresponding normal average. All of the data gap-filling and homogenization process was made with the `homogen` function of the `climatol` R package (Guijarro, 2024).

We summarized the homogenization parameters used for each step. Table A2 shows the parameters used to homogenize the monthly series, while Table A3 shows the parameters used to homogenize daily series by ecoregions 2, 3, 5, 6, and 7 and their corresponding subgroups.

A quality validation was performed using the McCuen test (McCuen, 2016) to ensure consistency during the data gap-filling process of the rainfall time series. McCuen test compares the differences between the aggregated rainfall of the original multi-annual monthly means and the final series. The generated rainfall time series with a difference greater than 10% related to its original was discarded.

Finally, to evaluate the effect of the gap-filling procedure on rainfall climatology, we calculated the root mean square error (RMSE) between the mean monthly precipitation of the original incomplete series and the corresponding completed series after gap filling. RMSE was calculated for each weather station and subsequently summarized by ecoregion and climate normal. This metric quantifies the deviation in the monthly climatological behavior introduced by the gap-filling procedure. Therefore, RMSE provides an indicator of the sensitivity of rainfall regimes to missing data completion across different climatic regions.

2.2 Identification of the best empirical relationships to estimate erosivity in Mexico

In this step, we identified the best empirical relationship to calculate the R factor according to the erosivity characteristics of Mexico. To achieve this, we evaluated three combinations of parameters $alpha$ and $beta$ in a power law model and used three databases with EI30 information on a global (Panagos et al., 2023), national Cortés (1991) and local (EI30 calculated from sub-hourly rainfall time series) scale.

2.2.1 Empirical relationships to estimate daily erosivity

The empirical relationship follows the power-law model proposed by Richardson et al. (1983) when using daily precipitation to estimate the daily erosivity R_d (Equation 1). When comparing rainfall erosivity estimates using power and linear models, power models perform better when applied to daily rainfall time series in tropical and subtropical zones (Rutebuka et al., 2020; Karami et al., 2012)

$$R_d = \alpha P_d^{\beta} \tag{1}$$

where P_d is the daily precipitation, α, and β are the adjusted coefficients. We tested three combinations (Model I, II, and III) of adjusted coefficients as follows:

- **Model I** (Richardson et al., 1983).

The value of α is equal to 0.18 for the cool season (October to March) and 0.41 for the warm season (April to September). The value of β is equal to 1.81 and constant throughout the year.

-**Model II** (Liu et al., 2020).

The value of α and β variate depending on the climate zone according to the Koppen-Greig Classification as follows: for Tropical (A), $\beta = 1.964 + 0.013 \times \text{Latitude}$, and $\alpha = 10^{(2.363-1.561\times\beta)}$. For Arid-steppe (BS), $\beta = 1.73$ and $\alpha = 0.3296$. For Arid-desert (BW), $\beta = 1.514$ and $\alpha = (2.123 - 0.04 \times \text{Latitude}) \times 10^{(1.781-1.341\times\beta)}$. For Temperate with dry summer (Cs), $\beta = 1.563$ and $\alpha = 0.2735$. For Temperate with dry winter (Cw), $\beta = 1.558$ and $\alpha = 0.817$. Finally, for Temperate with dry winter (Cf), $\beta = 1.5$ and $\alpha = (3.792 - 0.012 \times \text{Longitude} - 0.037 \times \text{Latitude}) \times 10^{(3.016-2.079\times\beta)}$. To identify the climate classification at each location of the datasets, we used the Koppen-Greig Classification for the present (1980-2016) at 1 km of spatial resolution made by (Beck et al., 2018).

-**Model III** (Xie et al., 2016).

The value of α is equal to 0.2686. The value of β is equal to 1.7265. This model also includes a sinusoidal relationship to describe the annual cycle of the coefficient of the power law function to represent seasonal differences in rainfall characteristics (Equation 2) as proposed by Yu and Rosewell (1996).

$$R_d = \alpha[1 + \eta cos(2\pi fj - \omega)]P_d^{\beta} \tag{2}$$

where f is the monthly frequency (1/12); ω is $7\pi/6$; η is 0.5412; and j is the j-month of the year.

2.2.2 Databases containing $EI30$ information

We used three databases to evaluate the performance of the three models described earlier. Two compiled databases provide $EI30$ values directly: a global dataset developed by Panagos et al. (2023) and a national dataset derived from the Master´s thesis of Cortés (1991). In addition, a local database was included to enable model performance at a finer scale in Mexico. This third database corresponds to the Michoacán Region and was constructed using sub-hourly (15 min) rainfall time series from which $EI30$ was calculated. These three validation databases have a different statistical distribution of the $EI30$ factor (Figure A1), displaying a wide range of values from 333 to almost 26000 MJ mm ha^{-1} h^{-1} yr^{-1}. Additionally, all validation databases show a strong linear relationship between the $EI30$ values and the mean annual rainfall (Figure A1b).

-GloREDa

On the global scale, the GloREDa database was built using data from almost 4000 weather stations worldwide (Panagos et al., 2023). They estimated the $EI30$ from rainfall time series with a resolution from 1 to 60 min. In Mexico, the GloREDa database has 15 locations with information on $EI30$ across continental territory (Figure 3a). The $EI30$ factor in these 15 locations was calculated from 5-minute rainfall time series from 2005 to 2015; however, not all the rainfall time series have registered for the multiyear period of ten years. The $EI30$ factor in this database shows a mean value of 3700.7 MJ mm ha^{-1} h^{-1} yr^{-1}, a standard deviation of 5719.2 MJ mm ha^{-1} h^{-1} yr^{-1}, and a range of 333.5 to 22743.6 MJ mm ha^{-1} h^{-1} yr^{-1}.

-Cortés

At the national scale, Cortés (1991) estimated the $EI30$ factor using 54 rainfall time series across Mexico (Figure 3b). The temporal resolution for those 54 rainfall time series is 1 minute, with a temporal period from 1977 to 1987. However, not all rainfall time series have registers for those ten years, so we selected 42 rainfall time series presenting more than five years of registers. The $EI30$ factor in this database shows a mean value of 4347 MJ mm ha^{-1} h^{-1} yr^{-1}, a standard deviation of 4827 MJ mm ha^{-1} h^{-1} yr^{-1}, and a range of 504 to 25654 MJ mm ha^{-1} h^{-1} yr^{-1}.

-**Michoacán** The Michoacán region is one of the main avocado-producing areas in Mexico, making it particularly relevant for studies of soil erosion in intensively managed agricultural systems. At the local scale, the Michoacán mountain region has a database with 30 rainfall time series (Figure 3c). These rainfall time series have a 15-minute temporal resolution, and the period of registers is from 2011 to 2017. The weather stations belong to the Association of Producers, Packers, and Exporters of Avocado from Mexico (APEAM). However, as finer time resolution is available in this case, we estimated the $EI30$ factor as defined in Wischmeier and Smith (1978) by using the `RainfallErosivityFactor` R package (Cardoso et al., 2020). The $EI30$ factor in this database shows a mean value of 10092 MJ mm ha^{-1} h^{-1} yr^{-1}, a standard deviation of 4928 MJ mm ha^{-1} h^{-1} yr^{-1}, and a range from 4580 to 22928 MJ mm ha^{-1} h^{-1} yr^{-1}.

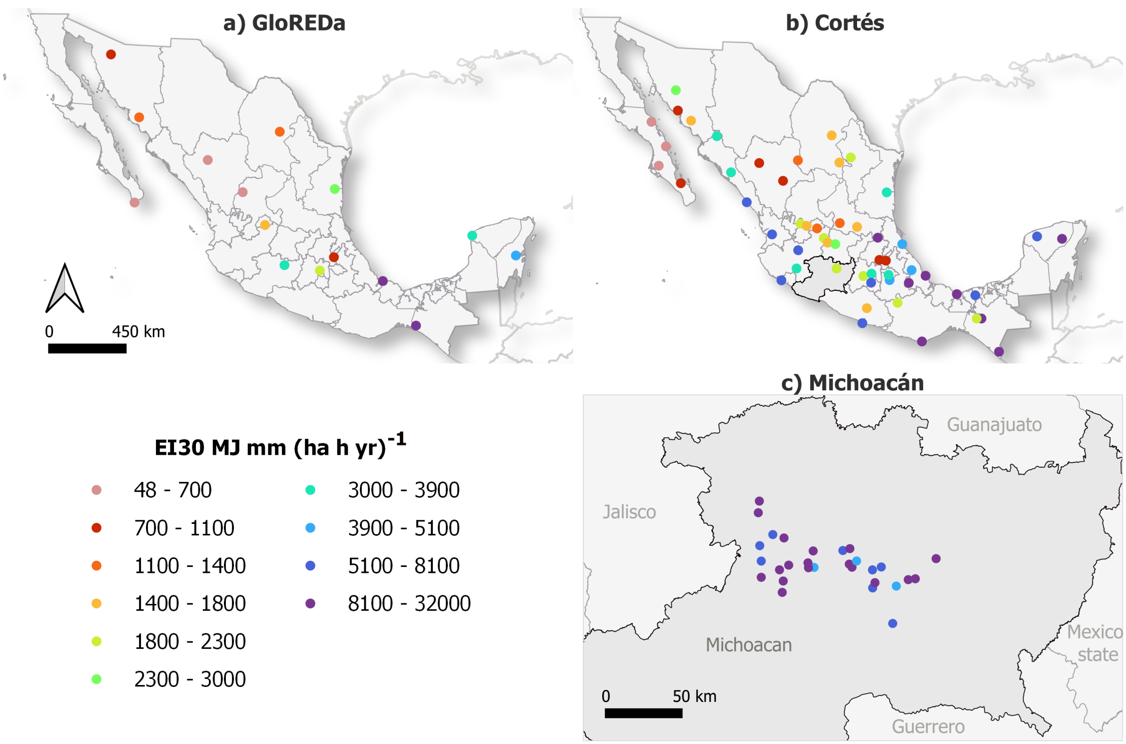

Figure 3. Spatial distribution of the validation datasets: a) GloREDa (n= 15), b) Cortés (n=44), and c) Michoacán (n=23).

2.2.3 Comparison of the empirical relationships

We compared the three $EI30$ databases against the R factor estimations by using the three coefficients (α and β) combinations called Model I, Model II, and Model III. We identified the direct comparison against the validation databases and our estimated Mexican databases (Mexico-CN1, Mexico-CN2, and Mexico-CN3) according to the overlapping between periods. Thus, the

GloREDa database was compared against the R factor calculated by using Mexico-CN3 (1988-2017). The Cortés database was compared against Mexico-CN1 (1968-1997) and Mexico-CN2 (1978-2007). and the Michoacán database was compared against Mexico-CN3 (1988-2017). Afterwards, for each point in the GloREDa and Cortés databases, we identified the nearest point in the Mexican database produced in this study. Moreover, as the Michoacán database is a 15-minute temporal resolution, we aggregated these rainfall time series at a daily resolution to estimate the R factor with the three coefficient combinations.

For those points in the Mexican databases, we calculated the daily erosivity R_d factor by using Model I, Model II, and Model III. Following, we calculated the annual erosivity R_y (MJ mm ha^{-1} h^{-1} yr^{-1}) as the sum of the daily erosivity values in a year (R_y=$\sum_{i=1}^{ed} R_{d_i}$). Finally, the R factor corresponds to the mean annual rainfall erosivity values for a multi-year period (R=$\sum_{j=1}^{30} R_{y_j}$).

We performed a linear regression to identify the relationship between the $EI30$ and R factor values. In this sense, the slope of the linear model quantifies the mean change in the R factor associated with a one-unit increase in $EI30$. Additionally, for each empirical model and validation database, we calculated the Mean Error (ME) and the Root Mean Square Error ($RMSE$) to evaluate the magnitude and direction of the differences between the estimated R factors and the observed $EI30$ values.

2.3 Rainfall erosivity estimation

We estimated the R factor for each weather station on the Mexican rainfall time series database. First, we identified the days with erosive rainfall as those with cumulative precipitation greater than 12.7 mm, an extension of the suggestion by (Wischmeier and Smith, 1978; Shin et al., 2019; Efthimiou, 2018). Second, we calculated daily erosivity R_d using the best coefficient combination identified in the previous step (sec. 2.2). Finally, we estimated the mean annual rainfall erosivity, R factor, as described in the previous step (sec. 2.2.3).

At this point, it is essential to highlight that we did not consider the erosivity due to the snowmelt because there is a pint-sized area covered with snow (or risk of snowfall), and no monitoring system for snowfall is publicly available in Mexico. To estimate the surface covered by snow, we explored the climate classification developed by García (1998), a modified Köppen classification system to better fit Mexico's climate conditions. According to the Köppen classification, only 83 km^2 (0.004% of the total area of Mexico) can be classified as E climates in the format of ET (tundra: temperature of warmest month greater than 0 °C but less than 10 °C) and EF (snow/ice: temperature of the warmest month 0 °C or below), both only produced by high altitudes. Additionally, the National Center for Disaster Prevention of Mexico developed a national snowfall danger index at a municipality level based on the occurrence of snowfall during the centuries XV to XXI (Jiménez Espinosa et al., 2012). They found that in the study period, snowfall had never occurred in 93.8% of Mexico's municipalities. Additionally, the municipality with the highest snowfall frequency is Juarez (Chihuahua state), with just 30 events over five centuries.

Finally, to provide an overview of the sensitivity associated with the gap-filling and homogenization procedures, the complete rainfall time series were modified according to the percentage change in the mean value of each rainfall time series before and after these procedures. As established in the quality control section (2.1.3), the mean change in the rainfall time series did not exceed 10%. The modified series were subsequently used to recalculate daily rainfall erosivity values, from which new R factors were estimated for each station and climate normal. The percentage change between the recalculated R factor and the R factor estimated from the complete rainfall time series after the gap-filling and homogenization procedures was then computed to evaluate the sensitivity of rainfall erosivity estimates to alterations introduced during these procedures. This analysis provides a first-order assessment of the propagation of uncertainties associated with modifications in the rainfall time series into long-term erosivity estimates.

At the end of this step, we obtained three datasets with R factor values for the three CNs: Mexico-CN1 (1968-1997), Mexico-CN2 (1978-2007), and Mexico-CN3 (1988-2017).

3 Results

This section presents the results of the three principal methodological stages outlined in the workflow. First, we developed a daily-resolution rainfall time series database, which provided a basis for further analysis. Second, we identified the best empirical relationship to estimated daily erosivity. Third, based on that best empirical relationship, we estimated rainfall erosivity values using the daily-resolution rainfall time series resulted in the first step.

3.1 Rainfall time series database development

The initial number of rainfall time series for the gap-filling, homogenization and quality control process was 1479, 1774, and 1721 for CN1, CN2, and CN3, respectively (Table 1). After data gap-filling, homogenization, and quality control, we discarded 4.8% of the rainfall time series. Hence, Table 1 shows that the largest number of rainfall time series corresponds to CN1 (1968-1997), with 7.4% (110 rainfall time series), which is followed by CN2 (1978-2007), with 5.4% (96 rainfall time series) and CN3 (1988-2017), with 2.6% (45 rainfall time series). Likewise, the most significant proportion of discarded rainfall time series corresponded to Mediterranean California (3 rainfall time series, 21.4%) and North American Deserts (29 rainfall time series, 15.84%) in CN1; Mediterranean California (2 rainfall time series, 11.11%) and Great Plains (7 rainfall time series, 12.72%) in CN2; and Great Plains (5 rainfall time series, 10.86%) in CN3. Additionally, in the data gap-filling processes, we identified that none of the 5 rainfall time series available for Mediterranean California, in CN3, had a rainfall register for three consecutive years, which did not allow us to carry out the data gap-filling process for the complete study period; however, CN1 and CN2 provide a robust basis for assessing rainfall erosivity in this ecoregion. Finally, we obtained a database with 1369, 1678, and 1676 rainfall time series for CN1, CN2, and CN3, respectively. The available rainfall time series are distributed across the Mexican territory for the three CNs and represent the seven ecoregions (Figure 4).

The percentage of variation of the series mean by ecoregion and CN using the two-step clustering is shown in Table 2. The CN2 (1978-2007) showed the highest average change in the mean, with -1.80%, where it is also noted that four of the seven ecoregions present relatively high average changes. Notably, in CN1 (1968-1997), for North American Deserts, the highest average change in the mean is -1.50%. In the CN3 (1988-2017), for Tropical Dry Forest and for Temperate Sierras, it is -3.38% and -1.61%, respectively. Additionally, Table A4 shows the Root Mean Square Error (mm) of the monthly accumulated rainfall by ecoregion. It can be seen that the highest RMSE was found for Tropical Rain Forest in the three CNs (6.12, 5.72, 6.78 mm, respectively), followed by Great Plains in CN2 and CN3 (5.72, 6.78 mm, respectively).

Table 1. Number of available rainfall time series before and after data gap-filling process, as well as the number of discarded rainfall time series. The frequency of the rainfall time series is shown by ecoregion and climate normal.

Ecoregion	RTS before data gap-filling process			RTS with change greater than 10%			RTS after the data gap-filling process		
	1968-1997	1978-2007	1988 - 2017	1968-1997	1978-2007	1988 - 2017	1968-1997	1978-2007	1988 - 2017
Mediterranean California	14	18	5	3	2		11	16	
North American Deserts	183	273	243	29	18	4	154	255	239
Semi-arid Elevations	248	314	322	5	12	5	243	302	317
Great Plains	38	55	46	3	7	5	35	48	41
Tropical Rain Forest	195	237	236	16	6	5	179	231	233
Tropical Dry Forest	401	466	454	26	25	12	375	441	444
Temperate Sierras	400	411	415	28	26	9	373	386	409
Total	**1479**	**1774**	**1721**	**110**	**96**	**40**	**1369**	**1678**	**1676**

Figure 4. Spatial distribution of the available weather stations for each climate normal: CN1 (1968-1997), CN2 (1978-2007), and CN3 (1988-2017).

Figure A2 shows the monthly rainfall distribution for the seven ecoregions for CN1 (1968–1997), CN2 (1978–2007), and CN3 (1988–2017). The results indicate that Mexico exhibits a unimodal rainfall regime, with a marked peak and a well-defined dry season across all ecoregions; however, the characteristics of the wet period vary among them. In the Tropical Rain Forest,

Table 2. Mean percentage change in the mean value of rainfall time series by ecoregion

	Ecoregion	Mean change in rainfall time series (%)		
		1968-1997	**1978-2007**	**1988 - 2017**
1	Mediterranean California	-0.84	3.24	
2	North American Deserts	-1.50	-1.36	-0.14
3	Semi-arid Elevations	-0.25	-1.37	0.03
4	Great Plains	-0.69	3.23	-0.29
5	Tropical Rain Forest	-0.06	0.20	0.10
6	Tropical Dry Forest	-0.54	-0.49	-3.38
7	Temperate Sierras	-0.20	-3.73	-1.61
	Total	-0.28	**-1.80**	-0.98

rainfall increases rapidly from May to June and peaks in September, with monthly values exceeding 300 mm. The Tropical Dry Forest and the Temperate Sierras show a similar annual pattern, with a persistent and evenly distributed wet season from June to September, reaching monthly values of around 200 mm. In the Semi-arid Elevations, the wet period begins in May, peaks in July (approximately 150 mm), and declines gradually until October. The Great Plains ecoregion exhibits a wet season that begins in March, followed by a gradual increase in rainfall, sustained precipitation through July (around 100 mm), and a peak in September (approximately 150 mm). In contrast, the North American Deserts ecoregion is characterised by low rainfall throughout the year, with only a modest increase during the summer months (around 50 mm), and no clear peak. The Mediterranean California ecoregion shows a markedly different pattern, with rainfall concentrated between November and March, reaching monthly values of approximately 50 mm. Overall, the general behavior of rainfall distribution across ecoregions is consistent among the three climate normals. However, slight differences are observed in CN3, where the North American Deserts show an increase in accumulated precipitation in September, and the Great Plains show an increase in July precipitation.

3.2 Identification of the best empirical relationships to estimate erosivity in Mexico

This section presents the results of identifying the best empirical relationship between $EI30$ and the R factor calculated from three models. To achieve this, we built linear models to identify the rate of change between the $EI30$ factor and the R factor estimated with the three models (Figure 5). In this context, a slope of 1 indicates perfect agreement between estimated R factors and $EI30$ values, whereas deviations from 1:1 slope reflect fewer agreement.

Model I was the coefficient combination with the best overall performance across the three datasets, with slopes closest to 1 (1.07, 0.92, 0.83, and 0.43 for GloREDa vs. Mexico-CN3, Cortés vs. Mexico-CN1, Cortés vs. México-CN2 and for the Michoacán database, respectively) and the lower RMSE values (1524, 2438, 2628, 4978 MJ mm ha^{-1} h^{-1} yr^{-1} for GloREDa vs. Mexico-CN3, Cortés vs. Mexico-CN1, Cortés vs. México-CN2 and for the Michoacán database, respectively). Whereas, Model II obtained the poorest performance for GloREDa vs Mexico-CN3, Cortés vs Mexico-CN1, and Cortés vs México-CN2

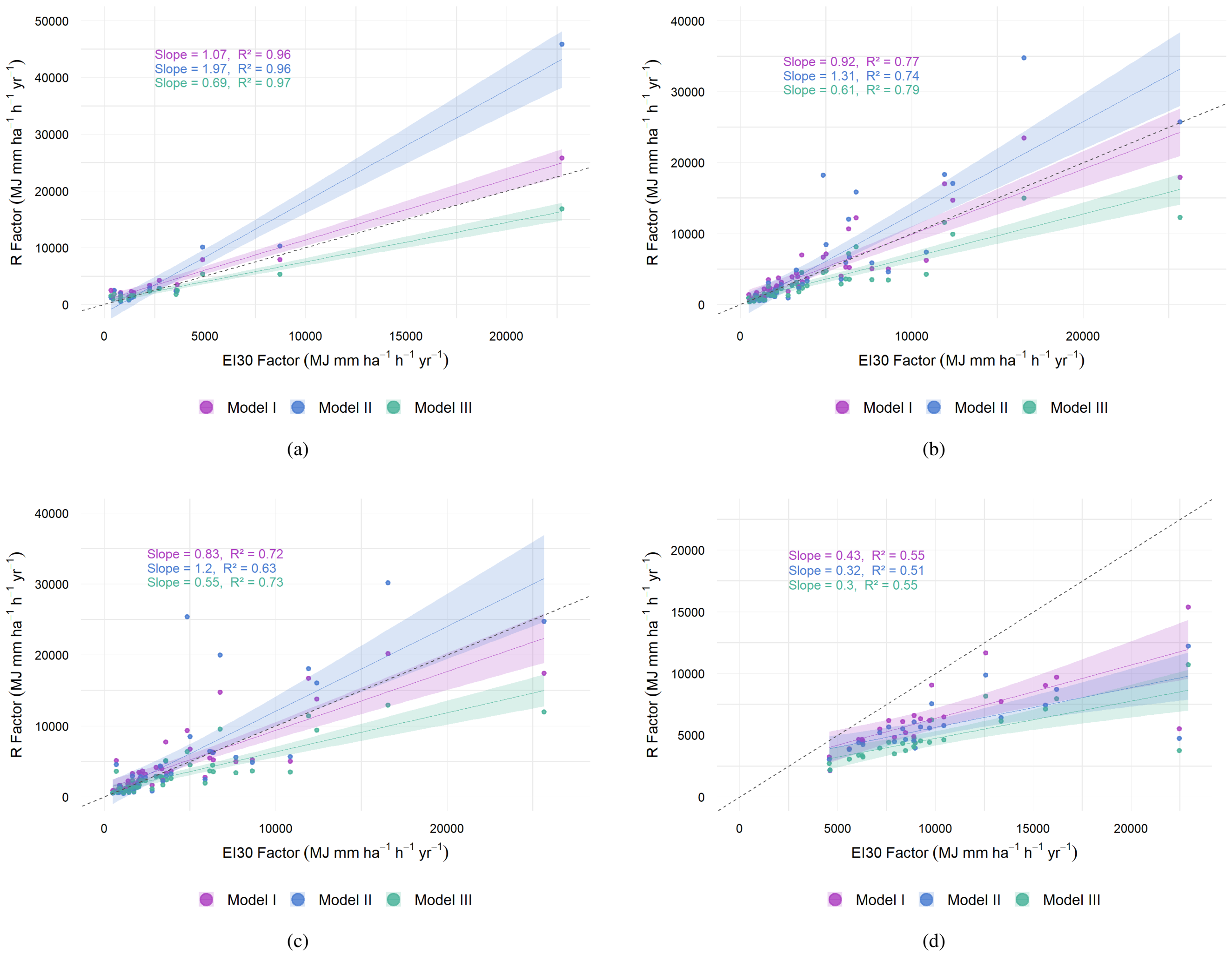

Figure 5. Comparison between observed $EI30$ factor and rainfall erosivity estimates (R) factor obtained using the three evaluated models across different datasets: (a) global (GloREDa), (b) national (Cortés; Mexico-CN1), (c) national (Cortés; Mexico-CN2), and (d) local (Michoacán). The x-axis represents observed $EI30$ values, while the y-axis shows model-based rainfall erosivity estimates derived from daily rainfall time series. Solid lines indicate the fitted linear regression for each model, and the dashed line represents the 1:1 relationship (perfect agreement). The slope of each regression is used as an indicator of model performance.

Table 3. Metrics of performance of three models: Model I (Richardson et al., 1983), Model II (Liu et al., 2020), and Model III (Xie et al., 2016) in predicting the $EI30$ values of three databases: GloREDa, Cortés and Michoacán. ME: Mean error and RMSE: Root Mean Square Error

Databases	**Models**	**Performance metrics MJ mm ha^{-1} h^{-1} yr^{-1}**	
		ME	**RMSE**
GloREDa vs. Mexico-CN3	I	956	1524
	II	2077	6176
	III	-566	1921
Cortés vs. Mexico-CN1	I	324	2438
	II	910	4088
	III	-1171	2667
Cortés vs. Mexico-CN2	I	338	2628
	II	959	4554
	III	-1153	2900
Michoacán	I	-3699	4978
	II	-4434	5717
	III	-5328	6438

with the highest RMSE values (6176, 4088, and 4554 MJ mm ha^{-1} h^{-1} yr^{-1}, respectively). Model III showed intermediate RMSE values, but consistently underestimated $EI30$ values in all datasets (negative ME values). For the Michoacán dataset, all three models underestimated $EI30$, with Model I still providing the best performance (ME = -3699; RMSE = 4978 MJ mm ha^{-1} h^{-1} yr^{-1}), followed by Models II and III, which showed progressively larger errors.

On the other hand, the distance of each point of the GloREDa and Cortés (Mexico-CN1 and Mexico-CN2) database to the nearest weather station varied in a range of 0.6 to 42.0 km (mean:11.6 km), 0.3 km to 73.4 km (mean: 12.17 km), and 0.3 to 76.5 km (mean: 10.7), respectively. It is important to highlight that there is no correlation between error and the distances between points in the validation datasets and the weather stations of our Mexican databases.

3.3 Rainfall Erosivity estimations

In this section, we present the results of rainfall erosivity estimates for the three climate normals considered. First, we describe the statistical distribution of erosivity values, followed by their annual distribution and, finally, their spatial distribution.

Figure A3 shows the mean number of locations with erosive rainfall for each day of the year for the three climate normals. In all CNs, erosive rainfall is concentrated within a single annual erosive season extending approximately from days 150 to 280, corresponding to the summer rainfall period in Mexico. For CN1, the erosive period is relatively stable, with the highest number of locations with erosive rainfall occurring between days 170 and 260. Similarly, CN2 exhibits a well-defined erosive season, although with slightly greater variability and higher peaks than CN1. In contrast, CN3 is characterised by a more pronounced intra-seasonal variability, with two distinct peaks occurring between days 173–190 and 229–261. These peaks correspond to periods when the number of locations reporting erosive rainfall exceeds the 90th percentile. Additionally, the 90th percentile threshold of the number of locations with erosive rainfall increases from 211 in CN1 to 227 in CN2 and 238 in CN3, representing increases of 7% and 12%, respectively, relative to CN1.

The mean values of rainfall erosivity for CN1, CN2, and CN3 were 5276 (SD 5662), 4832 (SD 5266), and 5067 (SD 5071) MJ mm ha^{-1} h^{-1} yr^{-1}, respectively (Table 4). The statistical distribution of the rainfall erosivity values was right-skewed with skewness of 2.7, 3.0, and 2.9 for CN1, CN2, and CN3, respectively. So the median was less than the mean with values of 3245, 3070, and 3327 MJ mm ha^{-1} h^{-1} yr^{-1} for CN1, CN2, and CN3, respectively. The Krustal-Wallis test showed that the erosivity median value for CN2 differed from CN1 and CN3 at a 95% confidence level. The kurtosis values of 12.6, 15.1, and 15.3 for CN1, CN2, and CN3, respectively, indicate large tails with the presence of outliers. In this case, the outliers are high erosivity values reaching more than 12000 MJ mm ha^{-1} h^{-1} yr^{-1} for the three CNs (Figure A4).

Table 4. Descriptive statistic of the erosivity values for three climate normals (1968-1997, 1978-2007, 1988-2017). Min: minimum, Max:maximum, SD: standard deviation, CV: coefficient of variation, skew: skewness, kurt: kurtosis

Climate normal	n	Mean	Median	SD	Min	Max	CV	Skew	Kurt
CN1 (1968-1997)	1369	5276	3245a	5662	65.5	49129	1.1	2.7	12.6
CN2 (1978-2007)	1678	4832	3070b	5265	56.8	44660	1.1	3.0	15.1
CN3 (1988-2017)	1676	5067	3327a	5071	64.2	43368	1.0	2.9	15.3

Monthly erosivity varies throughout the year in the three CNs (Figure 6a). The behavior of the erosivity in the three CNs is monomodal, indicating just one peak and one valley. The month with the highest erosivity is September, reaching values almost to 1300 MJ mm ha^{-1} h^{-1} yr^{-1}, followed by August, July, and June with erosivity values around 1000 MJ mm ha^{-1} h^{-1} yr^{-1}. It is important to highlight that for June, July, and August, the CN1 (1968-1997) had the highest monthly erosivity values; however, for September, the highest values are found in the CN2 (1988-2017). The months with the smallest erosivity values are February, followed by March with values less than 40 MJ mm ha^{-1} h^{-1} yr^{-1}.

As the three CNs had the same behavior throughout the year, we displayed in Figure 6b the monthly erosivity for CN3 by ecoregion. The Tropical Rain Forest exhibits the highest erosivity values throughout the year, ranging from a minimum in March (114 MJ mm ha^{-1} h^{-1} yr^{-1}) to a maximum in September (3395 MJ mm ha^{-1} h^{-1} yr^{-1}). In contrast, the North American Deserts show the lowest erosivity values, generally remaining below 500 MJ mm ha^{-1} h^{-1} yr^{-1}. Most ecoregions reach their maximum erosivity in September; however, the Semi-arid Elevations peak earlier, in July. It is important to note that CN3 does not include stations in the Mediterranean California ecoregion. Nevertheless, in CN1 and CN2, this ecoregion shows the lowest erosivity values among all regions.

Regarding the spatial distribution, the erosivity values across Mexican territory look similar for the three CNs (Figure 7 and A5). Low erosivity values (< 1000 MJ mm ha^{-1} h^{-1} yr^{-1}) are mainly concentrated in the Baja California peninsula and northern Mexico, corresponding to arid regions such as the North American Deserts and Semi-arid Elevations. Intermediate values (ap-

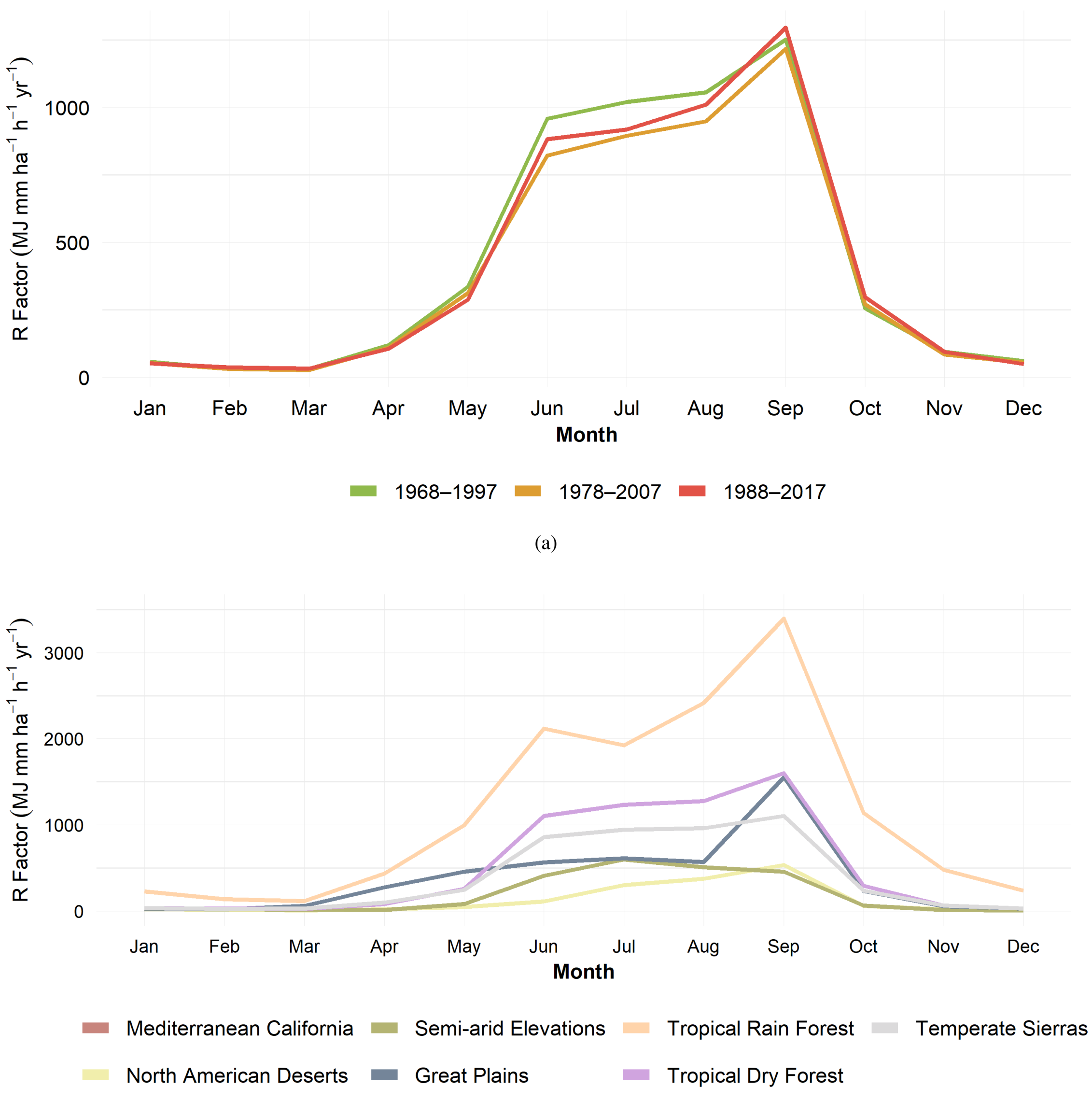

(a)

(b)

Figure 6. Montly erosivity values estimated from daily rainfall time series and using the Richardson et al. (1983) power-law model. a) Monthly erosivity for the three climate normals; b) Monthly erosivity by ecoregion for the Mexico-CN3 (1988-2017).

proximately 1600–4300 MJ mm ha^{-1} h^{-1} yr^{-1}) are distributed across central Mexico, reflecting transitional climatic conditions. In contrast, the highest erosivity values (> 7600 MJ mm ha^{-1} h^{-1} yr^{-1}) are concentrated in the southern and southeastern regions of the country. These areas correspond to the upper deciles of the statistical distribution, indicating a strong spatial concentration of high erosive potential in humid tropical environments. This spatial pattern is also reflected in the mean erosivity values calculated for each ecoregion (Table A5). The Tropical Rain Forest consistently exhibited the highest mean erosivity values for the three climate normals, followed by the Tropical Dry Forest, Temperate Sierras, and Great Plains. In contrast, the Mediterranean California and North American Deserts ecoregions showed the lowest mean erosivity values. Across the three climate normals, the relative hierarchy among ecoregions remained similar, with tropical and humid regions presenting substantially higher erosivity values than arid and semi-arid regions.

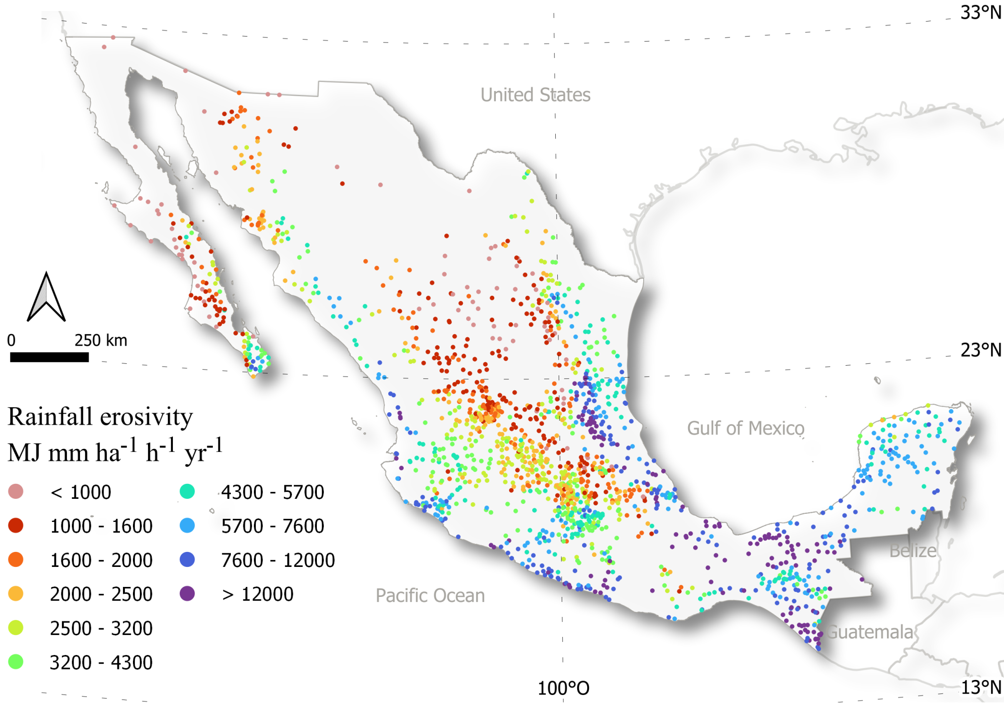

Figure 7. R factor values calculated with the power law equation proposed by (Richardson et al., 1983) at daily resolution for the climate normal 1988 - 2017. The legend classes approximately represent deciles of the statistical distribution, although not exactly.

The spatial distribution of percentage changes in rainfall erosivity after the homogenization and gap-filling procedures was heterogeneous across the three climate normals, with positive and negative changes interspersed throughout Mexico (Figure 8a for the CN3 and Figure A6a for the CN1 and CN2). In all climate normals, most stations exhibited relatively small changes, generally between -5% and 5%. CN1 showed a slight predominance of positive changes in northern Mexico, particularly in the Baja California Peninsula and northwestern regions, whereas CN2 displayed a more balanced distribution of positive and negative changes across the country. In contrast, CN3 exhibited a greater occurrence of negative changes in northern and northwestern Mexico. Southern Mexico and the Yucatán Peninsula generally showed lower magnitudes of change across the three climate normals. Overall, the largest positive and negative changes were associated with isolated stations rather than coherent regional clusters.

The scatterplots reveal a consistent inverse relationship between the percentage change in the mean rainfall series after the homogenization and gap-filling procedures and the corresponding percentage change in rainfall erosivity across the three climate normals (Figure 8b for the CN3 and Figure A6b for the CN1 and CN2). The three climate normals exhibited a similar funnel-shaped distribution, in which the dispersion of erosivity changes increased progressively as the magnitude of rainfall change became larger. Stations with precipitation changes close to 0% showed relatively small erosivity variations concentrated near zero, whereas stations with larger positive or negative rainfall changes exhibited a wider range of erosivity responses, reaching approximately ±20%.

Table A5 summarizes the percentage changes in rainfall erosivity by ecoregion for the three climate normals after the homogenization and gap-filling procedures. Overall, mean percentage changes remained low across all ecoregions and climate normals, with most values below 3%. For CN1, the largest mean positive percentage changes were observed in the North American Deserts (2.3%) and Mediterranean California (2.1%). In CN2, mean percentage changes were generally smaller, although the North American Deserts still exhibited the largest positive mean change (1.7%), while the Great Plains showed a slight negative mean change (-0.6%). Similarly, in CN3, mean percentage changes remained close to zero across ecoregions, ranging from -0.4% in the North American Deserts and Great Plains to 0.7% in the Tropical Dry Forest. Although the mean changes were comparatively small at the ecoregional scale, some individual stations exhibited larger positive and negative percentage changes. The maximum positive changes reached 21.2%, 19.3%, and 17.6% for CN1, CN2, and CN3, respectively, whereas the minimum changes reached -18.8%, -23.0%, and -19.3%. Overall, the range of percentage changes was similar among the three climate normals, with both positive and negative changes occurring within comparable magnitudes.

4 Discussion

This research addressed the data incompleteness and breakpoints in the legacy Mexican climate time series. Particularly, we compiled and systematised a national dataset with daily rainfall and rainfall erosivity for three climate normals (CN1:1968-1997, CN2:1978-2007, and CN3:1988-2017) across Mexico. To the best of our knowledge, this research is the first effort to develop a large daily rainfall time-series and erosivity dataset at the national scale, based on legacy climate data, following the quality-control and inhomogeneity analyses proposed by the World Meteorological Organization. This discussion is organised into four principal components. First, we discuss the development and quality-control procedures of the first national rainfall time series database for Mexico, including the implications of homogenization across contrasting climatic regions. Second, we analyse the rainfall erosivity estimates, their spatial patterns, and the performance of the empirical models used for daily erosivity estimation. Third, we evaluate the sensitivity of rainfall erosivity estimates to the homogenization and gap-filling

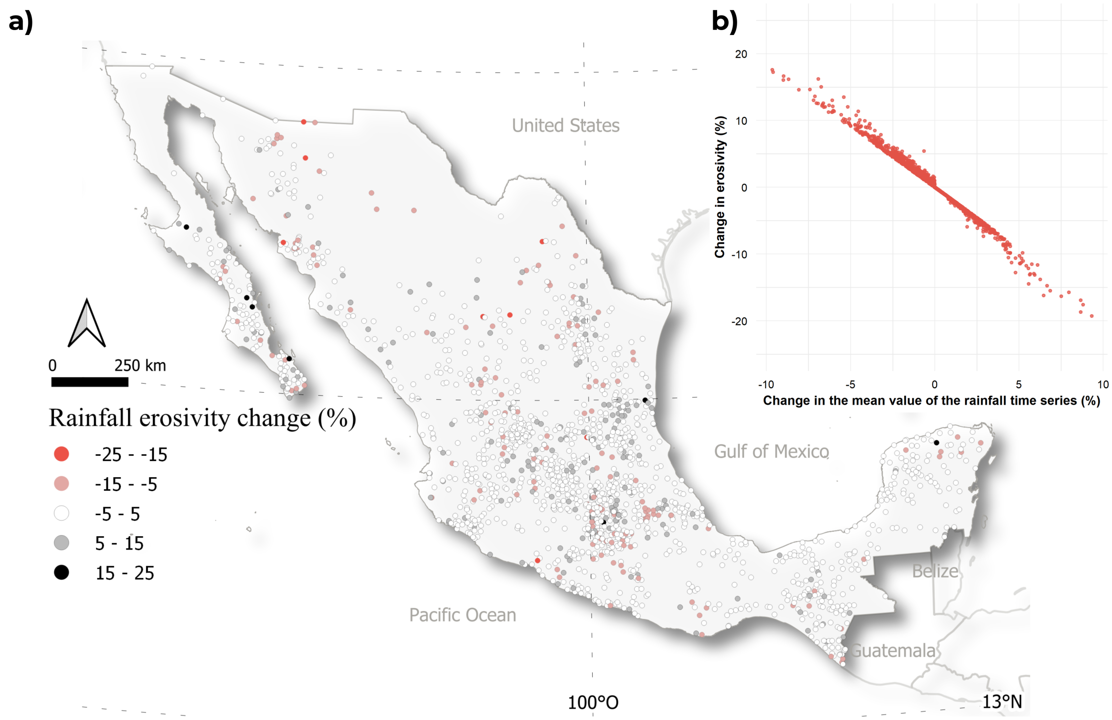

Figure 8. Percentage changes in rainfall erosivity after modifying precipitation time series according to the percentage change in the mean value of the rainfall time series before and after the gap-filling and homogenization processes for the 1988–2017 climate normal. a) Spatial distribution of percentage changes in rainfall erosivity. b) Relationship between percentage changes in the mean value of the rainfall time series and percentage changes in rainfall erosivity.

procedures. Finally, we discuss the limitations, potential applications, and future research directions associated with the rainfall and erosivity databases

4.1 Development of the first Mexican rainfall time series database

- Improvement over the previous rainfall products in Mexico

Previous national-scale rainfall datasets for Mexico are those produced by Cuervo-Robayo et al. (2014) and Carrera-Hernández (2025); they emphasise spatial completeness through interpolation. (Cuervo-Robayo et al., 2014) updated the mean monthly rainfall for 100 years (1910–2009) using around 5000 rainfall time series and used thin-plate smoothing spline interpolation to generate gridded data at 30 arcsec spatial resolution for the continental area of Mexico. Similarly, (Carrera-Hernández, 2025) developed the Mexico High Resolution Climate Database (MexHiResClimDB), a gridded dataset that provides daily, monthly, and annual rainfall for the period 1951–2020, using up to 4000 rainfall records per day. This dataset was generated using Kriging with External Drift on a local neighbourhood, producing gridded data at 20 arcsec spatial resolution across Mexico.

These approaches prioritise spatial completeness and provide valuable insights into the spatial distribution of climate variables across Mexico. However, previous gridded datasets either did not perform quality control (Cuervo-Robayo et al., 2014) or applied only basic quality control procedures (Carrera-Hernández, 2025), such as selecting stations with more than 80% of recorded data for at least 10 consecutive years and discarding unrealistic values (e.g., daily rainfall exceeding 600 mm).However, climatological studies have shown that inhomogeneities in rainfall time series can introduce biases and artificial trends, potentially leading to erroneous interpretations and misleading conclusions (Adeyeri et al., 2017). In consequence, WMO (2017, 2023) guidelines recommend that rainfall data undergo a comprehensive set of quality control tests, including constraint, consistency, rapid change, and domain analysis. These procedures are essential to ensure the reliability of climatic analyses, avoid biases due to measurement or recording errors, and maintain comparability across stations and regions, particularly in long-term rainfall time series.

Therefore, although gridded datasets are important for understanding large-scale ecological processes across Mexico, generating climate data from reliable and quality-controlled time series is equally important. This represents a key strength of our rainfall dataset compared to previous efforts. By providing a robust and quality-controlled rainfall time series database, we ensure greater reliability for climate analyses that depend on the accurate representation of extreme events and temporal variability, including rainfall erosivity estimation, hydrological modeling, and climate extremes assessment.

- Changes in the mean monthly rainfall by ecoregion

Since the homogenization process corrects outliers, artificial breaks, and inconsistencies in the raw records, larger RMSE values may reflect stronger corrections applied to low-quality or highly inhomogeneous rainfall series (Adeyeri et al., 2022). In this sense, the RMSE partly reflects the initial quality of the raw rainfall time series rather than solely the uncertainty introduced during the reconstruction process. Consequently, the RMSE also provides insight into the importance of homogenization and quality-control procedures across ecoregions, where breakpoints and outliers may affect rainfall series differently depending on the climatic regime. For example, in the Tropical Rain Forest ecoregion, the RMSE value for October was 12.11 mm, whereas the corresponding mean monthly precipitation was 230.9 mm, representing a relative deviation of only 5.4% with respect to the raw series. In contrast, in the North American Deserts, the RMSE value for March was only 2.08 mm; however, because the corresponding mean monthly precipitation was 7.97 mm, this represented a relative deviation of 26%. These comparisons indicate that rainfall series without homogenization may produce proportionally larger distortions in climatic variability and long-term trend analyses in arid and semi-arid regions, where low rainfall magnitudes amplify the effect of outliers and artificial breaks. This is particularly relevant because arid and semi-arid regions represent approximately 41.7% of the continental area of Mexico.

- Rainfall patterns across Mexico

The rainfall patterns observed across ecoregions are clearly influenced by both global climate dynamics and local topographic conditions. Overall, Mexico exhibits a unimodal rainfall regime, with a wet period occurring during late spring and summer (May to October), as reported by Carrera-Hernández (2025). However, the characteristics of this rainfall regime vary among ecoregions. For example, in the Tropical Dry Forest and Temperate Sierras (principally located over the Sierra Madre Occidental and the Eje Neovolcánico), the rainy season is concentrated between July and September. This pattern is largely driven by the North American Monsoon, which develops from July to September and originates along the western coast of Mexico (Gochis et al., 2006). During this period, a pressure gradient draws warm, moist air inland from the Pacific Ocean and the Gulf of California, and winds transport this moisture toward the interior. As the air rises over the Sierra Madre Occidental, it cools and condenses, producing convective rainfall, typically in the afternoon (Boos and Pascale, 2021). In addition to the monsoonal influence, the Tropical Rain Forest (located mainly in southeastern Mexico) exhibits a rainfall pattern associated with the northward migration of the Intertropical Convergence Zone, enhanced convective activity, and the contribution of tropical cyclones during late summer (August and September), resulting in increased monthly precipitation (de Anda Sánchez, 2020).

In contrast to the tropical and monsoonal processes that dominate rainfall across most of Mexico, the Mediterranean California rainfall pattern is influenced by different climate dynamics. This ecoregion is located in the northwesternmost part of Mexico (Figure 1) and is characterised by hot, dry summers and wet winters (García, 1998). Winter rainfall is associated with frontal storms originating in the Pacific Ocean (Deitch et al., 2017), linked to the position of the region on the equatorward flank of mid-latitude storm tracks and the poleward edge of the Hadley cell. In contrast, dry summer conditions are related to descending air and atmospheric subsidence associated with the eastern flanks of subtropical anticyclones (Seager et al., 2019).

4.2 Rainfall erosivity estimates and model performance

- Evaluation of empirical models for daily erosivity estimation

Among the three coefficient combinations evaluated for estimating daily rainfall erosivity, the Richardson et al. (1983) proposal consistently demonstrated superior performance across the national and local datasets. Although all three models adopt a similar functional structure of the form $R = \alpha P^{\beta}$, differences in the parameterisation of the α and β coefficients have substantial implications for model behavior under diverse rainfall regimes. The Richardson et al. (1983) equation was developed using rainfall time series across the United States of America, including rainfall conditions of the southern states such as Georgia, Mississippi, and Texas. This equation defines different α coefficients for the cool and warm seasons that occur from October to March and from April to September, respectively; it is very similar for the Mexican climate, where it is seen that the warmest months are those from May to October (Carrera-Hernández, 2025). Additionally, the β coefficient has no spatial or seasonal pattern, the same as found in the Xie et al. (2016) equation and contrary to the Liu et al. (2020) one, where the β coefficient is affected by the latitude in the Tropical (A) climate classification according to Köppen–Geiger. However, it is notable that the β coefficient for Richardson et al. (1983) equation (1.81) is slightly higher than that for Xie et al. (2016) and Liu et al. (2020) (1.72 and between 1.5 and 2 depending on the latitude, respectively), placing greater weight on high rainfall amounts which may better capture the erosive potential of intense storms. Indeed, this is the reason why the Richardson et al. (1983) model obtained the highest erosivity estimations for the Michoacán dataset (purple points always over the blue and green dots in Figure 5d), because β coefficients for all the Michoacán dataset were 1.81, 1.558 and 1.72 for the three models Richardson et al. (1983), Liu et al. (2020), and Xie et al. (2016), respectively.

- Erosivity estimations

Our work reveals that the distribution of erosivity values in Mexico corresponds to the geographical distribution of rainfall and seasonal precipitation conditions. The areas with the highest erosivity values are concentrated in the Isthmus of Tehuantepec (i.e., the shortest distance between the Gulf of Mexico and the Pacific Ocean). This region corresponds to the Tropical Rain Forest ecoregion, where high moisture availability enhances extreme precipitation events, increasing rainfall erosivity (Wang et al., 2023b). High values are also concentrated along the Pacific coastal zone and in low-elevation areas of the Sierra Madre Occidental, where previous studies have reported intense precipitation events at hourly and daily timescales (Gochis et al., 2006). In contrast, lower erosivity values occur in the central and northern regions of Mexico, where severe droughts (e.g., those occurring from the 1990s to the beginning of the twenty-first century), associated with large-scale ocean–atmosphere circulation patterns, have reduced mean annual rainfall. We also highlight a hotspot in the southern part of the Baja California Peninsula (e.g., Sierra La Laguna), where erosivity values are higher than those estimated for the northern part of the peninsula. This local variation is associated with the influence of tropical cyclones, which contribute up to 50% of the mean annual rainfall in this region (Agustín Breña-Naranjo et al., 2015). Overall, the spatial variability of erosivity across Mexico reflects the interplay between rainfall regimes and climatic events, underscoring the strong influence of regional atmospheric processes on soil erosion dynamics.

In agreement with these spatial patterns, our rainfall erosivity estimates are generally higher than those reported for Mexico by global products such as GloRESatE (Das et al., 2024) and GloREDa (Panagos et al., 2017). The GloRESatE grid reports erosivity values ranging from 49 to 49,811 MJ mm ha^{-1} h^{-1} yr^{-1}, with the highest values located in southern Chiapas. Similarly, the GloREDa grid reports values between 51 and 13,058 MJ mm ha^{-1} h^{-1} yr^{-1}, identifying the highest erosivity in the Isthmus of Tehuantepec and the coastal zone of the Gulf of Mexico. In contrast, our database reports maximum erosivity values exceeding 43,000 MJ mm ha^{-1} h^{-1} yr^{-1} in the tropical regions of southern Mexico. Additionally, Tong et al. (2026) reported erosivity values ranging from 8,000 to 20,000 MJ mm ha^{-1} h^{-1} yr^{-1} for the Yucatán Peninsula, further supporting the occurrence of high erosivity conditions in tropical regions of Mexico.

Despite differences in magnitude, both global products and our dataset consistently identify tropical regions as the areas with the highest erosivity. This pattern is also consistent with the global distribution of EI30 values reported in the databases used to construct these products. For example, the GloRESatE database (Das et al., 2024), which contains approximately 6200 sites worldwide, reports a maximum EI30 value of 39,124 MJ mm ha^{-1} h^{-1} yr^{-1} in Bangladesh. Likewise, the GloREDa database (Panagos et al., 2017), based on 3940 sites globally, reports a maximum erosivity value of 58,288 MJ mm ha^{-1} h^{-1} yr^{-1} in Las Cruces, Costa Rica. These comparisons suggest that the high erosivity values observed in tropical regions of southern Mexico are consistent with the global tendency for extreme erosivity to occur in humid tropical environments.

Conversely, the lowest erosivity values in our database are associated with the arid regions of northern Mexico and are consistent with those reported by GloREDa and GloRESatE. Although there are no specific EI30 estimations available for these Mexican arid regions, comparable values have been reported for the southern United States, which shares similar climatic conditions. For example, Kim et al. (2020) estimated EI30 values between 500 and 1000 MJ mm ha^{-1} h^{-1} yr^{-1} using CMORPH satellite data with a temporal resolution of 30 minutes and a spatial resolution of 8 km. Similarly, the GloRESatE database

(Das et al., 2024), which includes a large number of weather stations across the United States, reports erosivity values ranging from 400 to 1200 MJ mm ha^{-1} h^{-1} yr^{-1} near the Mexico–United States border. These comparisons indicate that the low erosivity values identified in northern Mexico are consistent with the broader climatic conditions of arid and semi-arid regions in North America.

- Improvement over previous erosivity datasets.

This new erosivity dataset is appealing due to two principal advantages: spatial and temporal coverage. It provides erosivity values for a substantially larger number of sites (1369, 1678, and 1676 for CN1, CN2, and CN3, respectively) compared to the dataset developed by Panagos et al. (2023), which includes erosivity estimates for 15 sites in Mexico, and the dataset compiled by Cortés (1991), which estimated erosivity values for only 53 sites across the country. Additionally, this dataset improves the representation of rainfall erosivity conditions in several regions, particularly in the north of Mexico (e.g., Chihuahua and Baja California), the central region (e.g., Zacatecas and Querétaro), and the south (e.g., Campeche and Quintana Roo), where erosivity estimates were previously unavailable. Additionally, this database provides erosivity estimations for the most rainy regions in Mexico, such as the Pacific coast and the isthmus of Tehuantepec

On the other hand, this database is appealing for presenting multi-annual erosivity values for three climate normals covering the period from 1968 to 2017. As defined by Wischmeier and Smith (1978), estimating the R factor requires a long-term rainfall time series for reasonable estimations. Some studies have reported different minimum length required for a reliable estimations of rainfall erosivity: five years (Wang et al., 2024), 10 years (Verstraeten et al., 2006), 15 years (Hanel et al., 2016), and 20 years (Vantas et al., 2019; Renard and Freimund, 1994). In contrast, previous datasets have reported erosivity estimations from rainfall time series with a length between 1 and 11 years (Cortés, 1991) and 5 and 10 years in Panagos et al. (2023). This new database is appealing for the need of long-term rainfall time series to mitigate the seasonal and cyclical rainfall biases in the estimation of rainfall erosivity (Kumar et al., 2026).

- Sensitivity of R-factor estimates to homogenization and gap filling process.

To evaluate the implications of the homogenization and gap-filling procedures on rainfall erosivity estimates, we analyzed both the sensitivity of erosivity responses to changes in the rainfall time series and the spatial distribution of these changes across Mexico. The results reveal that homogenization may locally modify erosivity estimates; however, the spatial structure of rainfall erosivity patterns remains consistent across ecoregions. The funnel-shaped distribution observed in the scatterplots (Figures 8b and A6b) indicates a high sensitivity in the erosivity estimations to the larger changes in the mean of the rainfall time series (Pianosi et al., 2016). This sensitivity is explained by the potential model implemented in erosivity estimation (Xie et al., 2016), but it could also partly be explained by changes in the number of erosive rainfall days. Since daily erosivity was calculated only for days exceeding the erosive rainfall threshold (12.7 mm), modifications introduced during homogenization and gap filling may cause some days to move above or below this threshold. As a result, changes in rainfall can affect both the magnitude of daily erosivity and the frequency of erosive days, leading to greater dispersion in erosivity responses as rainfall changes become larger.

The absence of spatially coherent clusters of positive or negative erosivity change suggests that the effects of the homogenization and gap-filling procedures were not primarily controlled by regional climate conditions. This is particularly relevant because the gap-filling process was performed within ecoregions, using neighbouring stations in the same climatic context (Adeyeri et al., 2022). Therefore, if the procedure had introduced a systematic regional bias, changes would be expected to appear spatially concentrated within specific ecoregions. Instead, the largest changes occurred at isolated stations, suggesting that they are more likely associated with the initial quality of individual non-homogenized rainfall time series. In this sense, larger percentage changes in the mean of the rainfall time series should be interpreted as indicators of stronger corrections applied to the raw rainfall time series, rather than as evidence of systematic distortion introduced by the homogenization process. Thus, the spatially scattered distribution of changes supports the interpretation that the homogenization procedure corrected station-specific inconsistencies while preserving the broader ecoregional rainfall structure.

4.3 Limitations and potential use of the study

- Limitations of the rainfall and erosivity database

Models based on coarser rainfall time series can underestimate and overestimate $EI30$ values, as observed in this study. Although calculated at a coarser temporal resolution, underestimations have already been indicated by Tu et al. (2023); Yin et al. (2015) while evaluating the effect of modifying the time interval for calculating $R(EI30)$ using 5, 15, 30, and 60-minute rainfall time series. The authors concluded that increasing the time interval leads to underestimating erosivity values. Similarly, Li et al. (2022) identifies that using a monthly model underestimates $R(EI30)$. However, the same author found an overestimation of the R values regarding $R(EI30)$ using annual models. However, no matter under or overestimation, it has been reported that when coarser time intervals are used instead of high temporal resolution, the relationship between E and $I30$ remains consistent, but a larger calibration coefficient is needed (Tu et al., 2023). Therefore, having more detailed information is arguably the best way to estimate the erosivity factor with greater certainty and to know which model explains the greatest variance of $R(EI30)$.

In this study, the best-performing coefficient combination was that proposed by Richardson et al. (1983). However, we did not differentiate parameter coefficients by ecoregion due to the limited availability of sites with $(EI30)$ values. In regions with high-intensity rainfall events, such as the Pacific coastal zone of Mexico, rainfall tends to exhibit greater erosivity than in regions with lower-intensity rainfall, even when total rainfall amounts are similar. Under these conditions, coefficient parameters are expected to vary across regions (Li et al., 2022; Chen et al., 2020), reflecting differences in the erosive power of rainfall. Additionally, the choice of model and its associated coefficients constitutes an important source of uncertainty in subsequent soil loss estimations, which should be taken into account by users (Li et al., 2022).

- Potential uses of the rainfall and erosivity database

This new database will help as an indicator of rainfall erosivity patterns across Mexico. We report daily rainfall at a wide range of altitudes from 1 to 4283 meters above sea level. This is a valuable rainfall database because it is meeting the three primary requirements to the Universal Soil Loss Equation (USLE) and its derived models: (1) estimation of average annual rainfall erosivity for predicting long-term soil loss; (2) construction of seasonal erosivity curves to reflect the interaction between rainfall distribution and crop management practices; and (3) calculation of daily or 10-year return period erosivity values to assess the impact of extreme events on runoff generation and the effectiveness of soil conservation measures, such as terracing Yin et al. (2017).

In this context, this erosivity database represents a valuable tool for local, national, and global erosion studies. At the local scale, it can support the design of field experiments to validate rainfall erosivity estimates under different rainfall regimes, as well as the identification of the magnitude of underestimation or overestimation associated with different temporal resolutions of rainfall data (Meng et al., 2021; Zhao et al., 2019; Dunkerley, 2019). Finally, because this database spans a long period (1968–2017) and is divided into three climate normals, it enables users to analyse trends in rainfall and rainfall erosivity values and relate them to other erosion drivers, such as land use and soil cover dynamics (Yan et al., 2014).

At the national scale, this database can be used as input for erosion models to establish a baseline of soil loss rates across Mexico; indeed, the need for reliable erosivity values has been highlighted in previous studies (Bolaños González et al., 2016). Additionally, within the framework of the United Nations Convention to Combat Desertification (UNCCD), countries have the opportunity to report their contributions to the Sustainable Development Goals (SDGs), including Indicator 15.3.1, which measures the proportion of degraded land relative to the total land area (Sims et al., 2021). In this context, Mexico could use this database to improve the assessment of such indicators by relying on nationally derived datasets, which better capture local conditions than global products.

At the global scale, this new erosivity database is appealing for validating global datasets that are generally used to evaluate soil erosion by water at large scales when no more detailed information is available, for example, the global rainfall erosivity databases such as GloREDa (Panagos et al., 2023, 2017) or the Global Rainfall Erosivity database from Reanalysis and Satellite Estimates -GloRESatE- (Das et al., 2024). The GloREDa is a gridded erosivity product (at 1 km spatial resolution) made with almost 4000 rainfall time series at 30-min temporal resolution to estimate $EI30$ values, and global bioclimatic covariates. Appealing for a validation of the use of this database, we compared our erosivity estimations with those published in Panagos et al. (2017).

We identified that our rainfall erosivity predictions for the Mexico-CN3 database obtained greater values than those from Panagos et al. (2017) product (dots under the 1:1 dashed line in Figure 9). The North American Deserts and the Semi-arid elevation ecoregions obtained similar erosivity estimations (yellow and green dots); in contrast, the Tropical Rain Forest and the Temperate Sierras were those ecoregions with the most significant differences between estimations (peach and gray dots). This difference in the Tropical Rain Forest (the wettest ecoregion) is evident because the ecoregion has higher mean annual rainfall and standard deviation (862 to 4823 mm and an SD of 758 mm). In comparison, the Panagos et al. (2017) reports a lower mean annual rainfall (1383-2100 mm and an SD of 402.35 mm, those values calculated with three rainfall time series in the ecoregion). The same pattern is observed for Temperate Mountains, where Mexico-CN3 has a wider probability distribution of mean annual rainfall (range of 318-4009 mm and an SD of 500 mm) than Panagos et al. (2017) (range of 814 to 2258 mm, in this ecoregion, GloREDa has just two rainfall time series). We therefore report a more complete description of rainfall time series variance. We believe that our contribution could be useful in better representing global erosivity estimates.

Consistent with our results, Fenta et al. (2023) found the largest differences in annual rainfall erosivity values between the global product and a satellite-based approach (using sub-hourly rainfall time series) in the rainiest regions (tropical and

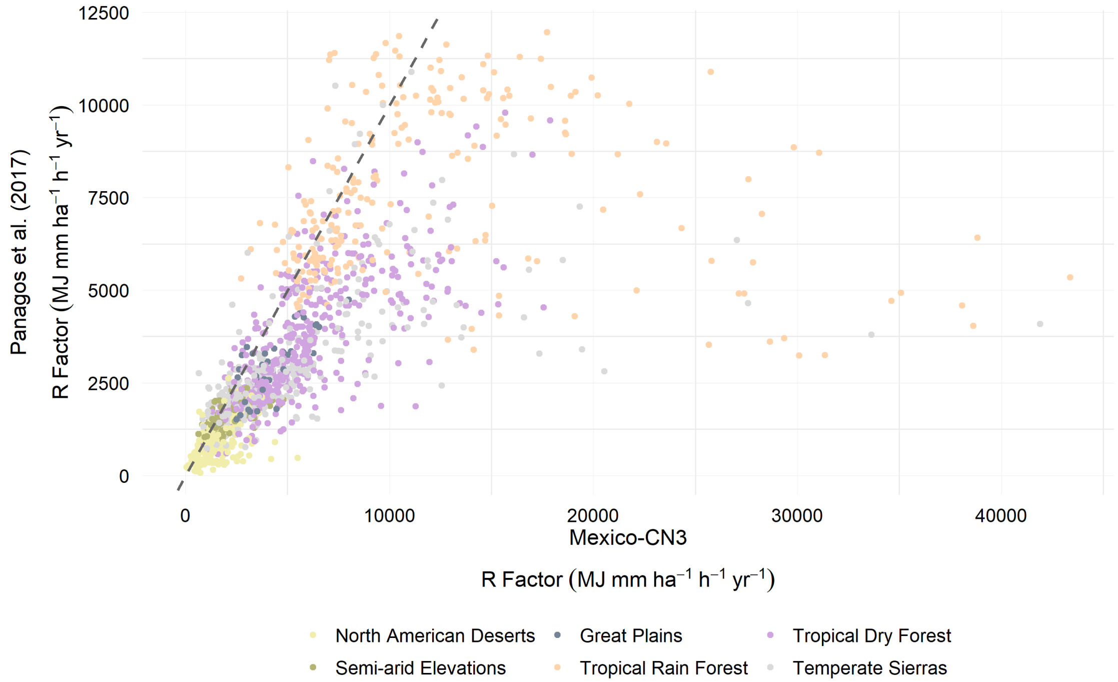

(a)

Figure 9. Scatter plot of R factor values from the global rainfall erosivity surface from Panagos et al. (2017) and the R factor estimated with the Richardson et al. (1983) power law equation with the rainfall time series of the Mexico-CN3 (1988-2017) database.

temperate climates) worldwide. The best agreement between satellite-based rainfall erosivity (using the satellite precipitation estimates corrected and reprocessed with the Climate Prediction Center Morphing Technique - CMORPH) and the Panagos et al. (2017) product was found in Europe, where the density of rainfall gauges is the highest globally (Bezak et al., 2022; Matthews et al., 2025). Furthermore, as the global product has in its database just 15 rainfall erosivity values in the Mexican area, it is important to identify the regions with high discrepancies between our national approach and the global product, to understand their limitations and use them in places with scarce rainfall erosivity information.

4.4 Future research directions

Now, we present our perspective on future directions for cost effective modeling and mapping rainfall erosivity patterns and trends across Mexico along with four main interoperability barriers: a) transitioning into high temporal resolution and to sub hourly dynamics, b) climate change projections and non stationarity, c) integration with digital soil mapping and soil organic carbon sequestration models and d) uncertainty quantification and the role of citizen science.

First, while the current database provides a robust baseline for the R-factor in Mexico, future research could prioritise the integration of sub-hourly rainfall intensity data. The increasing availability of automated weather station networks and high-resolution satellite products (such as GPM-IMERG) offers a pathway to characterise soil erosivity with increased accuracy

(Yin et al., 2017; Yan et al., 2025; Lobo and Bonilla, 2015). Transitioning from daily aggregates to event-based modeling will allow for a deeper understanding of how extreme, short-duration convective storms, which are common in Mexico's complex topography, contribute disproportionately to annual soil loss.

Second, rainfall erosivity projections are commonly based on stationarity assumptions (Vantas et al., 2020); a critical frontier involves the incorporation of non-stationarity into erosivity mapping. As climate change alters the frequency and intensity of tropical cyclones and North American Monsoon patterns, static historical averages may become less predictive (Almagro et al., 2017; Wang et al., 2023a; Zhang et al., 2010). Future modeling efforts could couple the current R factor baseline with CMIP6 climate projections to develop digital scenarios of future erosivity patterns and trends. This will be essential for designing long-term sustainable land management strategies and adapting hydraulic infrastructure to a more aggressive erosive environment.

Third, there is a significant opportunity to integrate rainfall erosivity databases with digital soil mapping frameworks to evaluate the positive and negative feedbacks between erosion and soil organic carbon dynamics (Song et al., 2026; Min et al., 2026; Qiao et al., 2025). Future studies could focus on the soil carbon losses in response to soil erosion and sediment transport across different geomorphic positions (Sun et al., 2024; Silva et al., 2016). By coupling high-resolution erosivity maps with national soil property grids, researchers can better quantify the role of water erosion in carbon redistribution, moving Mexico toward a more comprehensive National Soil Monitoring System (Abbruzzini et al., 2026; Guerrero et al., 2014; Varón-Ramírez and Guevara, 2024).

Fourth, future iterations of the Mexican rainfall erosivity database should focus on rigorous uncertainty quantification e.g., using Bayesian frameworks or ensemble modeling. Given the uneven distribution of primary weather stations across Mexico's complex and diverse terrain, identifying regions with high predictive uncertainty is paramount. Furthermore, the integration of 'Citizen Science' and low-cost IoT (Internet of Things) recording rain gauge could serve as a useful validation tool. Engaging local communities in data collection would not only fill geographic gaps but also bridge the divide between high-level modeling and on-the-ground soil conservation practices (Duwal et al., 2025; Dawoud et al., 2023; Tedla et al., 2022).

5 Conclusions

We present the first harmonized rainfall and rainfall erosivity database for Mexico, developed from legacy climate data and covering the period from 1968 to 2017. Our workflow included complete quality control and homogenization processes to ensure data quality for 1369, 1678, and 1676 rainfall time series data and rainfall erosivity for three climate normals (1968-1997, 1978-2007, and 1988-2017), respectively. This is a climatological database that substantially improves the spatial representation and documentation of erosivity patterns compared to global and local products.

Results revealed a strong climatic and geographical control on erosivity patterns. Tropical humid regions, particularly the Isthmus of Tehuantepec, southern Mexico, and portions of the Pacific coastal zone, exhibited the highest erosivity values, whereas the arid and semi-arid regions of northern Mexico showed the lowest erosive potential. These patterns are consistent with the broader global tendency for extreme erosivity to occur in humid tropical environments.

The sensitivity analysis indicates that the homogenization and gap-filling procedures may locally modify rainfall erosivity estimates, particularly in stations with low-quality or highly inhomogeneous rainfall records. However, despite these local variations, the general spatial patterns and ecoregional contrasts of rainfall erosivity remained stable across the three climate normals. These results suggest that the homogenization process effectively corrected station-specific inconsistencies while preserving the broader climatic structure of rainfall erosivity across Mexico

The new database provides an important foundation for national-scale soil erosion assessments and improves the representation of rainfall forcing for RUSLE-based applications, land degradation studies, hydrological analyses, and climate-related environmental research. In addition, the open availability of the database under FAIR principles facilitates its use by researchers, technical agencies, students, and decision-makers interested in rainfall dynamics and soil erosion processes in Mexico.

Future efforts should focus on incorporating high-temporal-resolution rainfall observations from automatic weather stations, strengthening institutional data-sharing initiatives, and developing spatially explicit erosivity prediction models using geostatistical and machine learning approaches. These advances would further improve the accuracy of rainfall erosivity estimation and contribute to more robust soil erosion assessments under changing climatic conditions.

6 Code availability

Rproject scripts to reproduce the workflow described in this research is available at: https://doi.org/10.5281/zenodo.15468097 (Varón-Ramírez, 2025)

7 Data availability

Following the FAIR principles for scientific data, we published the resulting rainfall erosivity databases (Mexico-CN1 1968–1997, Mexico-CN2 1978–2007, and Mexico-CN3 1988–2017) together with the completed daily rainfall time series for the three climate normals in the Environmental Data Initiative (EDI) repository at https://doi.org/10.6073/pasta/dd2b30e28ee25ff2d60d8a9f436951d2 (Varón-Ramírez et al., 2026).

The rainfall erosivity databases contain station metadata, including weather station code, name, geographic coordinates, altitude, and ecoregion, as well as indicators associated with the homogenization and gap-filling procedures, such as the Root Mean Square Error (RMSE) and the percentage change in the rainfall time series. Additionally, the databases include mean annual rainfall, the accumulated number of erosive rainfall days, and rainfall erosivity estimates derived from the empirical models proposed by Richardson et al. (1983), Liu et al. (2020), Xie et al. (2016).

The daily rainfall databases contain quality-controlled, homogenized, and gap-filled daily rainfall time series for 1369, 1678, and 1676 weather stations corresponding to the 1968–1997, 1978–2007, and 1988–2017 climate normals, respectively. Each rainfall time series is identified by a unique weather station code and includes flags associated with the quality-control and homogenization procedures.

Appendix A: Supplementary Tables and Figures

Table A1. Identification of the number of rainfall time series with consecutive zero and NA values

Consecutive years	**Number of RS with sequences of NA and zeros**			**Decision**
	1968 - 1997	**1978 - 2007**	**1988 - 2017**	
1	794	787	611	Not changed
2	344	478	613	Not changed
3	155	286	277	Replaced with NA and used as reference
4	88	136	109	Replaced with NA and used as reference
5	77	78	82	Replaced with NA and used as reference
6	21	11	31	Replaced with NA and used as reference
7	1	1	0	Removed
8	2	2	3	Removed
9	1	2	2	Removed
10	2	0	0	Removed
11	3	2	1	Removed
12	0	0	0	Removed
13	0	1	1	Removed
14	0	1	0	Removed
15	0	0	0	Removed
16	1	2	0	Removed
RS (NA menor 20%)	1489	1785	1728	
RS removed	10	11	7	
RS for data gap-filling process	1479	1774	1721	

Table A2. Homogenization parameters for monthly series. Eco: Ecoregion (1: Mediterranean California, 2: North American Deserts, 3: Semi-arid Elevations, 4: Great Plains, 5: Tropical Rain Forest, 6: Tropical Dry Forest, 7: Temperate Sierras); inht: threshold values used to identify break points in the Standard Normal Homogeneity Test (SNHT); dz.max and dz.min (upper and lower): standard deviations to consider suspicious and anomalous data.

Climate normal	Eco	inht	dz.max lower	dz.max upper	dz.min lower	dz.min upper
	1	15	8	10	-8	-10
	2	25	12	13	-7	-8
	3	40	10	11	-8	-9
1968 - 1997	4	20	6	7	-5	-6
	5	30	8	9	-6	-7
	6	30	14	16	-10	-10
	7	35	12	13	-7	-8
	1	15	10	10	-10	-10
	2	35	12	13	-8	-9
	3	35	11	12	-8	-9
1968 - 1997	4	20	8	9	-7	-8
	5	50	8	9	-7	-8
	6	30	13	14	-10	-11
	7	40	9	10	-8	-8
	1	–	–	–	–	–
	2	50	14	14	-10	-10
	3	60	14	14	-8	-8
1968 - 1997	4	15	7	7	-6	-6
	5	55	8	8	-7	-7
	6	60	14	14	-10	-10
	7	100	12	12	-8	-8

Table A3. Homogenization parameters for daily rainfall time series by ecoregion and group. Eco: Ecoregion (2: North American Deserts, 3: Semi-arid Elevations, 5: Tropical Rain Forest, 6: Tropical Dry Forest, 7: Temperate Sierras); RS: Number of rainfall time series; inht: threshold values used to identify break points in the Standard Normal Homogeneity Test (SNHT); dz.max and dz.min (upper and lower): standard deviations to consider suspicious and anomalous data

1968-1997

Eco	Group	RS	inht	dz.max lower	dz.max upper	dz.min lower	dz.min upper
2	1	94	50	40	45	-20	-20
	2	18	25	40	45	-25	-30
	3	36	20	40	45	-25	-30
	4	35	20	35	40	-20	-25
3	1	34	25	24	26	-10	-12
	2	87	40	26	28	-14	-16
	3	59	40	22	24	-12	-12
	4	52	40	26	28	-14	-14
	5	16	40	26	28	-10	-12
5	1	36	20	30	35	-15	-20
	2	11	5	20	22	-10	-10
	3	36	50	24	26	-14	-14
	4	58	50	30	32	-14	-16
	5	27	40	20	22	-10	-12
	6	27	40	20	22	-12	-14
6	1	118	25	35	40	-30	-30
	2	187	60	40	45	-25	-30
	3	77	25	40	40	-20	-25
	4	19	25	50	55	-30	-35
7	1	82	50	22	24	-14	-16
	2	49	50	35	35	-20	-25
	3	153	50	35	35	-25	-25
	4	116	50	24	26	-10	-12

1978-2007

Eco	Group	RS	inht	dz.max lower	dz.max upper	dz.min lower	dz.min upper
2	1	142	60	32	34	-18	-18
	2	23	20	45	50	-25	-25
	3	68	12	35	40	-30	-35
	4	40	12	30	35	-20	-25
3	1	41	30	22	24	-12	-14
	2	55	25	22	24	-14	-14
	3	130	50	24	26	-14	-14
	4	71	40	24	26	-12	-14
	5	16	30	22	24	-10	-12
5	1	42	40	30	35	-25	-30
	2	13	50	18	20	-10	-12
	3	30	40	18	20	-12	-14
	4	32	40	18	20	-16	-18
	5	68	50	22	24	-16	-18
	6	52	30	20	22	-12	-14
6	1	62	20	30	30	-20	-25
	2	267	80	30	35	-25	-30
	3	117	25	30	30	-25	-30
	4	20	10	40	45	-35	-35
7	1	87	60	20	22	-12	-14
	2	62	60	35	40	-25	-30
	3	157	80	26	28	-12	-14
	4	105	70	26	28	-22	-24

1988-2017

Eco	Group	RS	inht	dz.max lower	dz.max upper	dz.min lower	dz.min upper
2	1	112	100	40	45	-20	-25
	2	12	10	35	40	-25	-30
	3	45	20	35	40	-20	-25
	4	67	50	45	40	-30	-35
3	1	115	60	26	28	-16	-16
	2	27	20	22	24	-14	-14
	3	180	40	26	28	-18	-18
5	1	80	60	22	24	-20	-22
	2	81	40	24	26	-16	-18
	3	75	100	24	26	-16	-18
6	1	290	200	35	40	-25	-30
	2	46	20	30	35	-20	-25
	3	85	80	35	40	-30	-35
	4	33	15	40	45	-35	-40
7	1	242	250	26	28	-14	-14
	2	59	100	35	40	-25	-25
	3	114	200	30	35	-25	-30

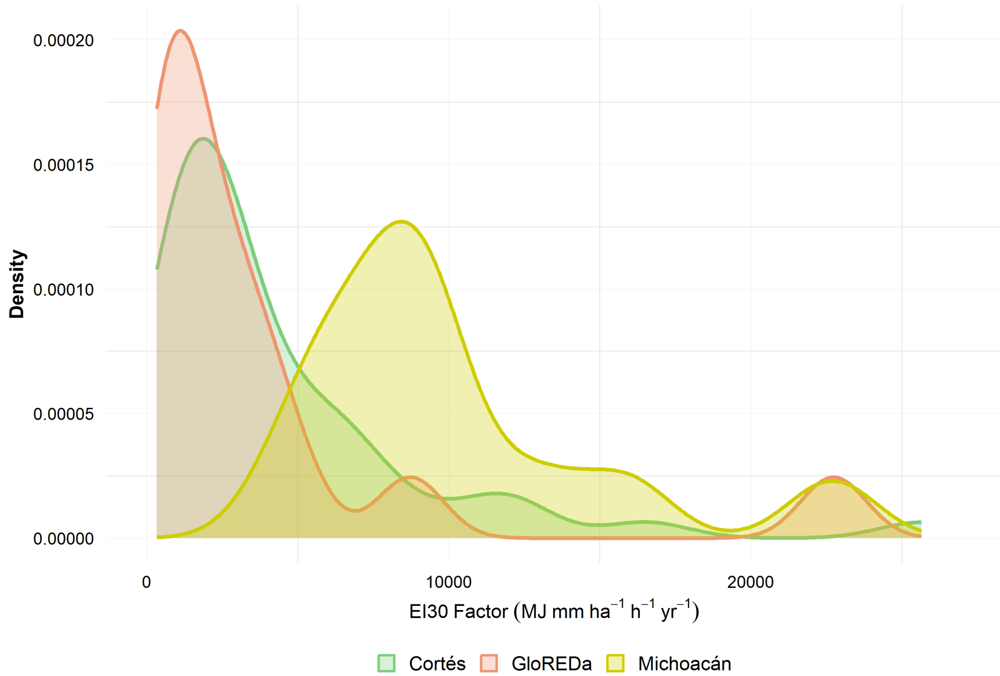

(a)

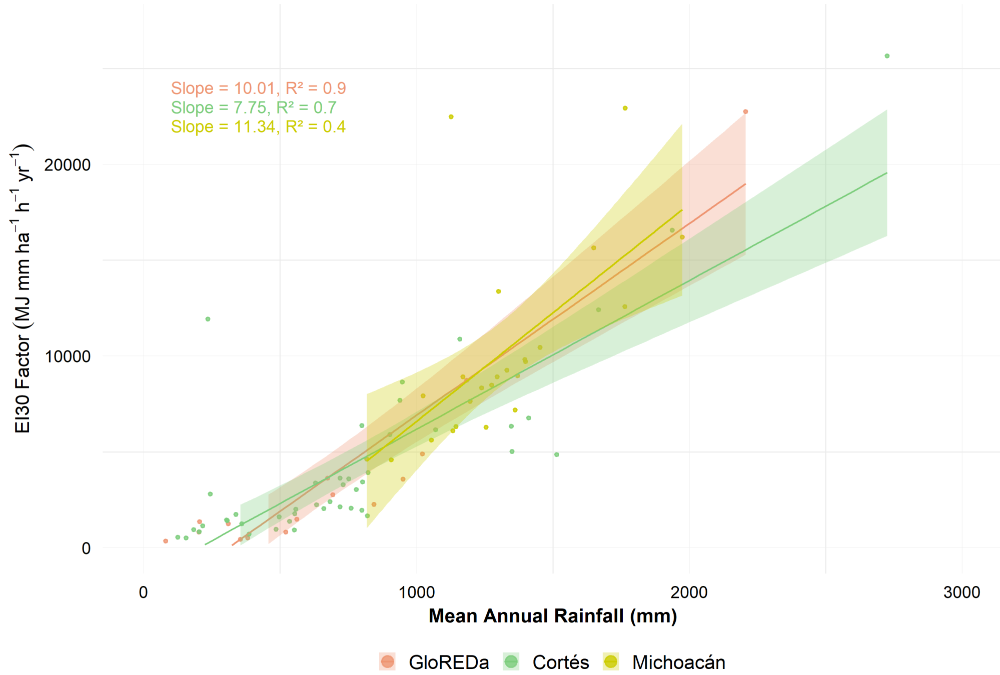

(b)

Figure A1. Characteristics of the three validations databases: GloREDa, Cortés, and Michoacán. a) Density plot of $EI30$ values; b) Linear relationship between $EI30$ and the mean annual rainfall

Table A4. Monthly climatological deviation introduced by the gap-filling process by month and ecoregion (metric RMSE in mm). Eco: Ecoregion (1: Mediterranean California, 2: North American Deserts, 3: Semi-arid Elevations, 4: Great Plains, 5: Tropical Rain Forest, 6: Tropical Dry Forest, 7: Temperate Sierras)

Climate Normal	Eco	Jan	Feb	Mar	Apr	May	Jun	Jul	Aug	Sept	Oct	Nov	Dec	Total
	1	6.84	6.71	6.10	1.36	0.33	0.16	0.67	0.58	0.60	0.78	1.74	3.43	2.44
	2	1.91	1.39	1.02	1.31	1.37	2.20	6.32	3.42	3.55	2.84	1.11	2.41	2.40
	3	1.83	0.96	0.93	0.78	1.42	3.08	3.64	3.15	3.06	1.85	0.74	0.83	1.86
1968-1997	4	1.72	2.08	1.06	2.25	2.66	3.61	1.74	4.40	3.75	2.62	1.02	1.63	2.38
	5	3.07	3.57	4.28	3.20	6.06	7.92	8.39	8.45	9.79	8.32	5.66	4.78	**6.12**
	6	2.47	1.17	1.49	1.46	2.75	6.26	6.76	5.84	7.13	3.90	2.34	1.89	**3.62**
	7	2.31	1.07	1.53	2.06	2.75	4.55	5.11	5.00	8.03	3.93	2.11	2.06	3.38
	1	8.16	5.81	7.87	1.63	0.86	2.53	0.41	1.40	0.70	1.73	3.27	5.69	3.34
	2	2.13	1.13	0.86	1.38	1.73	1.98	5.26	3.95	3.84	2.10	1.06	2.28	2.31
	3	1.66	0.93	0.75	0.72	1.38	3.54	3.73	3.21	3.49	1.81	0.75	0.95	1.91
1978-2007	4	2.77	1.95	1.97	3.44	3.27	5.06	6.15	5.68	9.01	5.08	1.55	3.40	**4.11**
	5	4.04	3.82	3.15	3.02	6.01	7.71	6.34	7.07	8.66	9.14	5.22	4.51	**5.72**
	6	3.19	1.12	0.92	1.68	2.89	6.83	5.71	5.71	8.58	4.85	2.38	2.38	3.85
	7	2.37	1.31	1.17	2.35	4.08	5.61	6.34	5.54	6.92	6.92	2.72	2.27	3.97
	2	1.59	1.45	2.08	1.11	2.02	2.14	6.21	3.96	4.88	2.53	1.89	2.69	2.71
	3	1.67	1.68	1.23	0.77	1.41	3.23	4.29	4.56	3.21	1.99	1.05	1.11	2.18
	4	2.75	2.53	4.08	6.08	8.74	5.68	13.17	9.87	12.52	6.27	5.05	6.27	**6.92**
1988-2017	5	5.25	3.48	3.21	3.42	6.81	7.79	8.51	9.69	9.06	12.11	7.34	4.73	**6.78**
	6	3.56	1.68	1.57	2.38	3.48	6.35	6.55	6.78	8.28	5.42	2.41	2.36	4.24
	7	2.73	2.28	2.55	2.21	6.34	6.79	8.65	7.59	8.34	6.08	4.37	3.20	5.09
Total		3.10	2.31	2.39	2.13	3.32	4.65	**5.70**	**5.29**	**6.17**	4.51	2.69	2.94	**3.77**

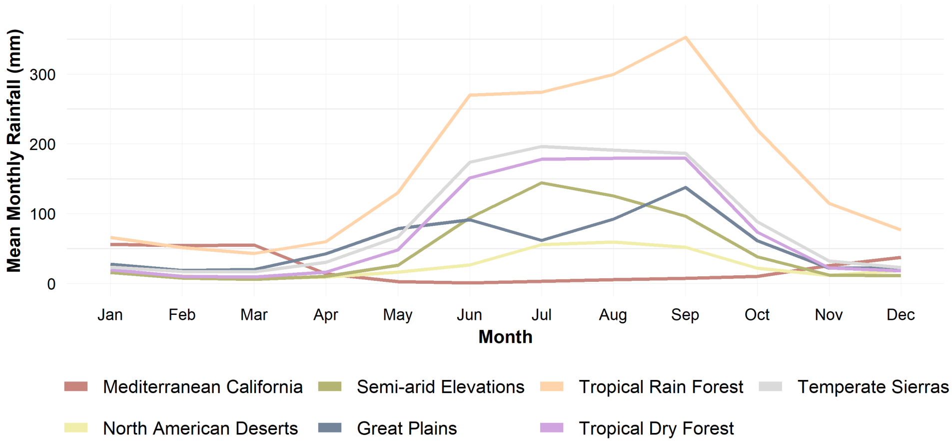

(a)

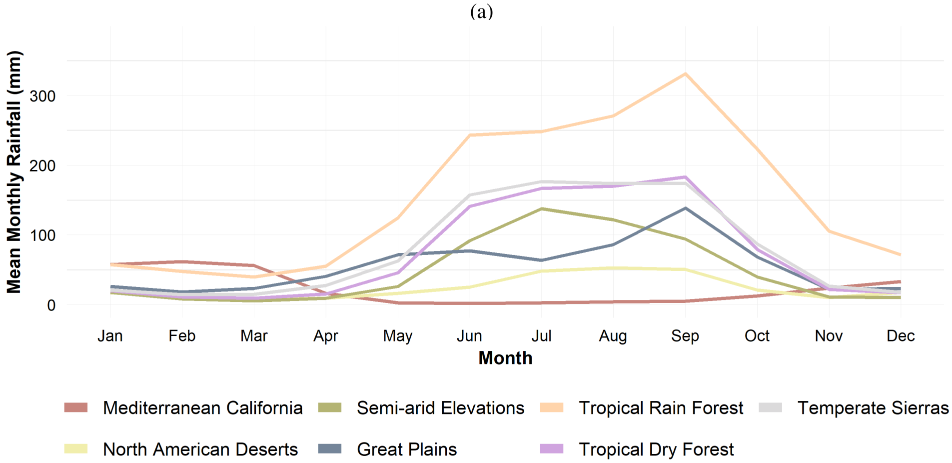

(b)

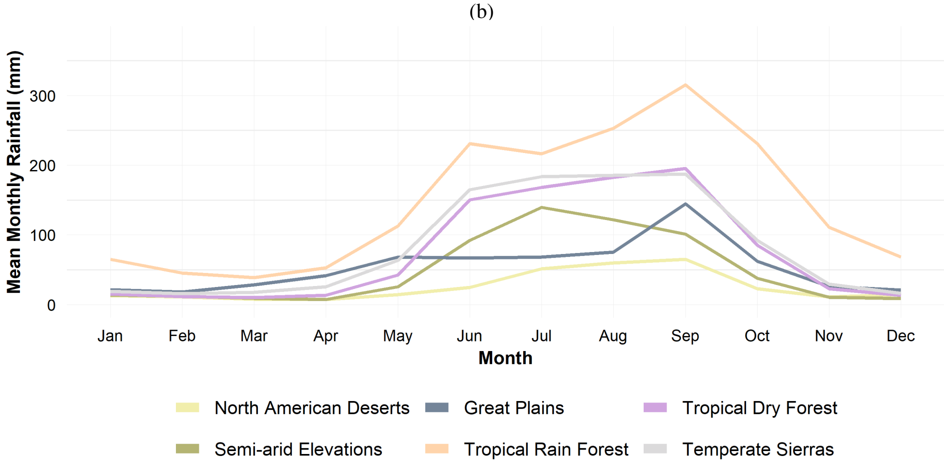

(c)

Figure A2. Mean monthly rainfall for all seven ecoregions. a) Climate normal (CN1) 1968-1997; b) Climate normal (CN2) 1978-2007; and c) Climate normal (CN3) 1988-2017

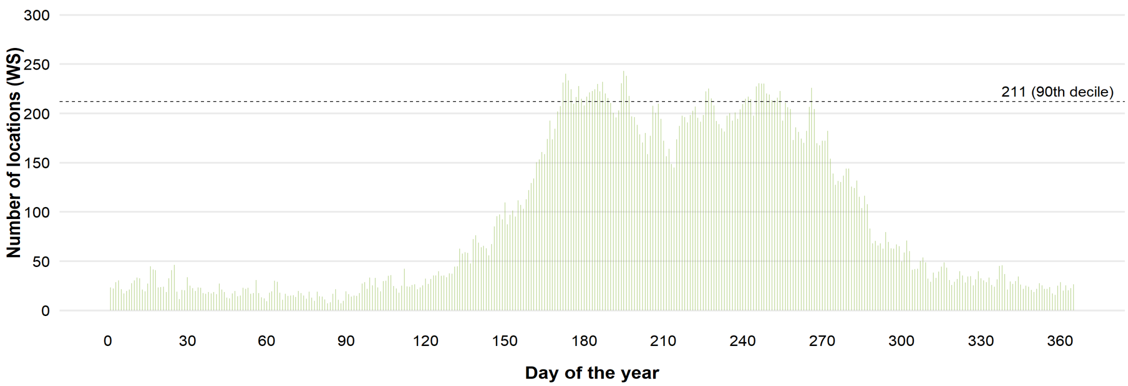

(a)

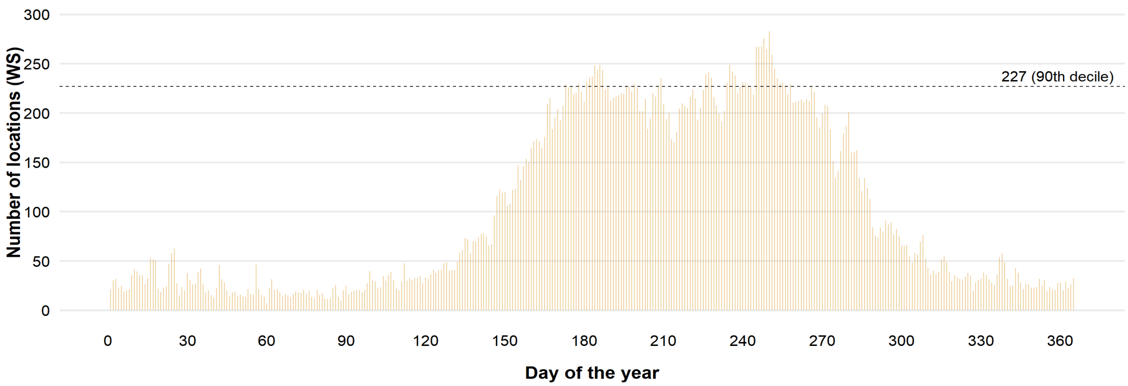

(b)

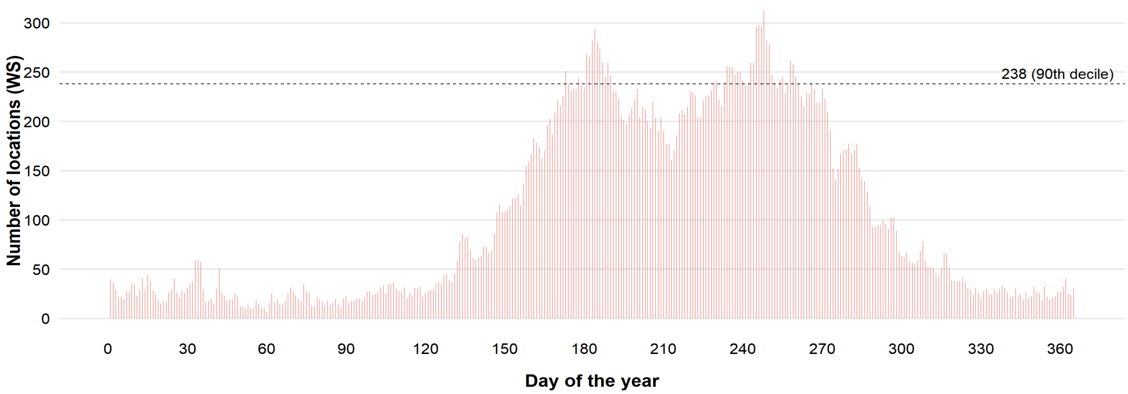

(c)

Figure A3. Number of locations with erosive rainfall of each day of the year for the three climate normal, a) 1968-1997, b) 1978-2007, and c) 1988-2017

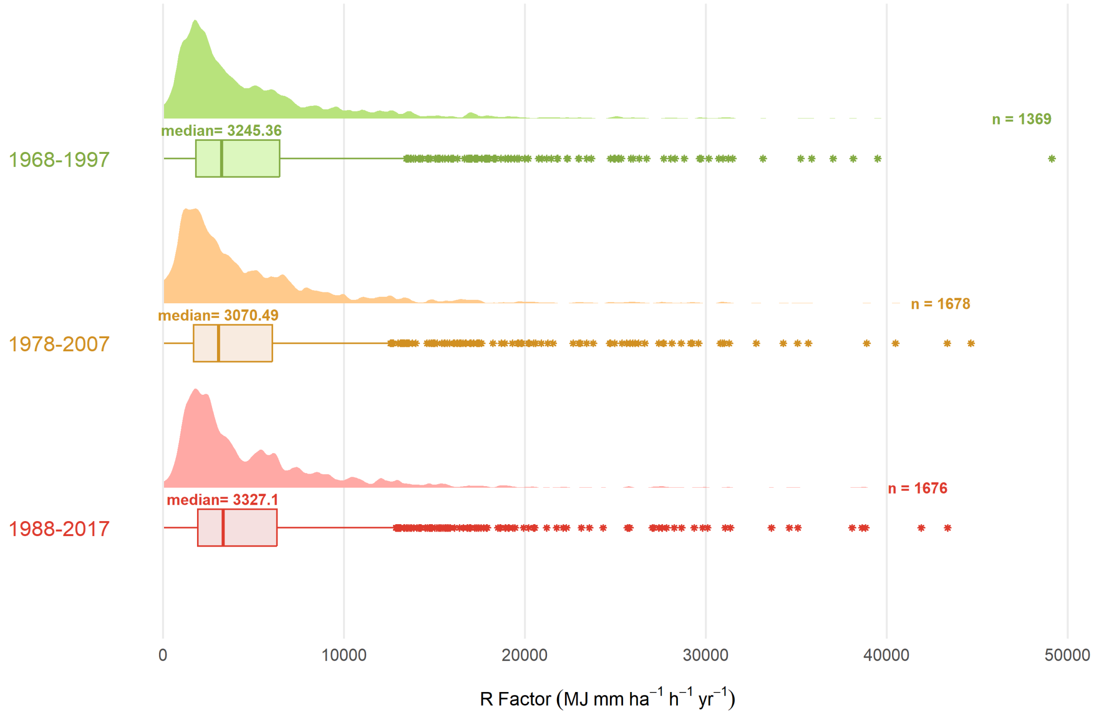

Figure A4. Density plot and Box-Plot of erosivity factor (R) calculated from daily rainfall time series for the three climate normals

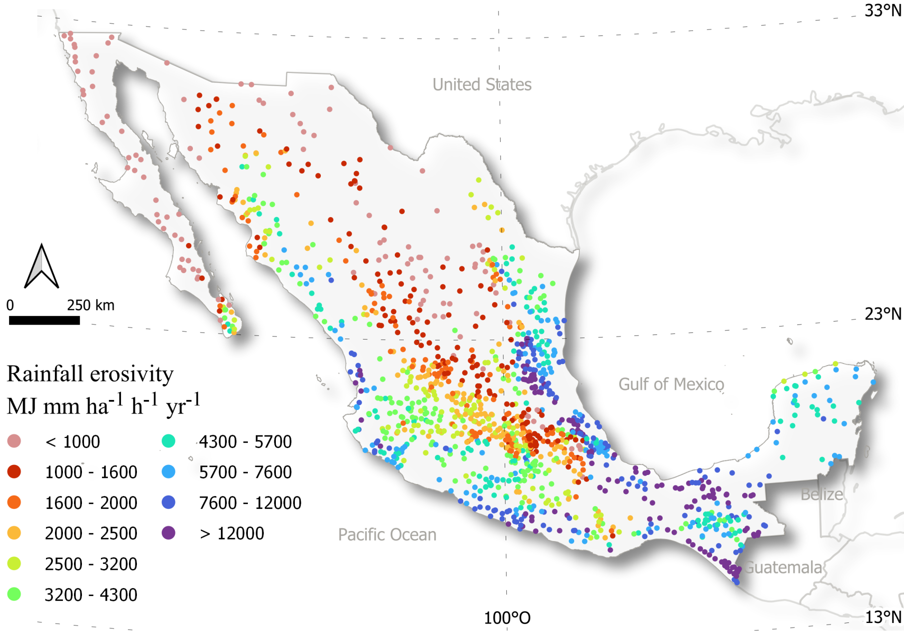

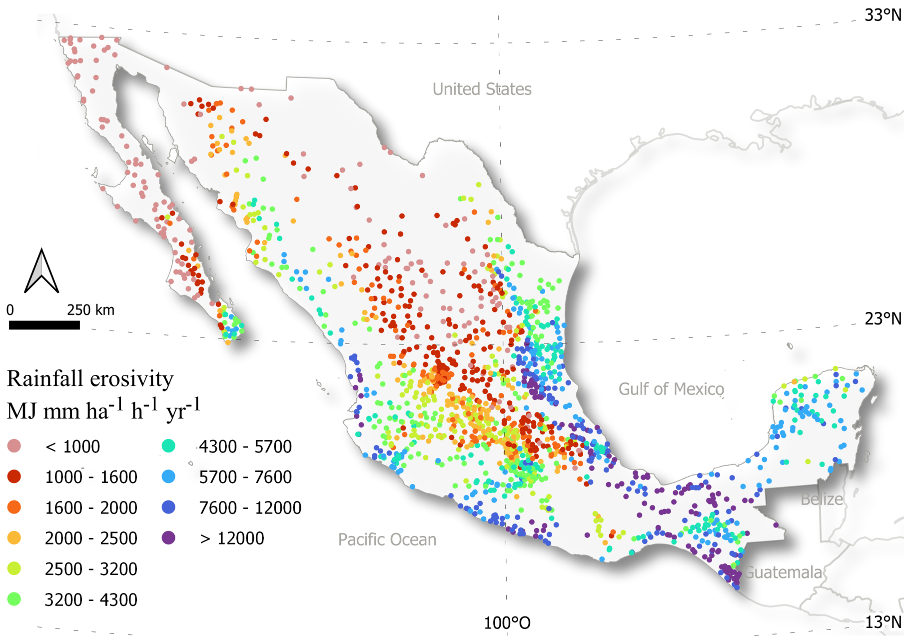

Figure A5. R factor values calculated with the power law equation proposed by (Richardson et al., 1983) at daily resolution. Upper panel: climate normal 1968–1997. Bottom panel: climate normal 1978–2007. The legend classes approximately represent deciles of the statistical distribution, although not exactly

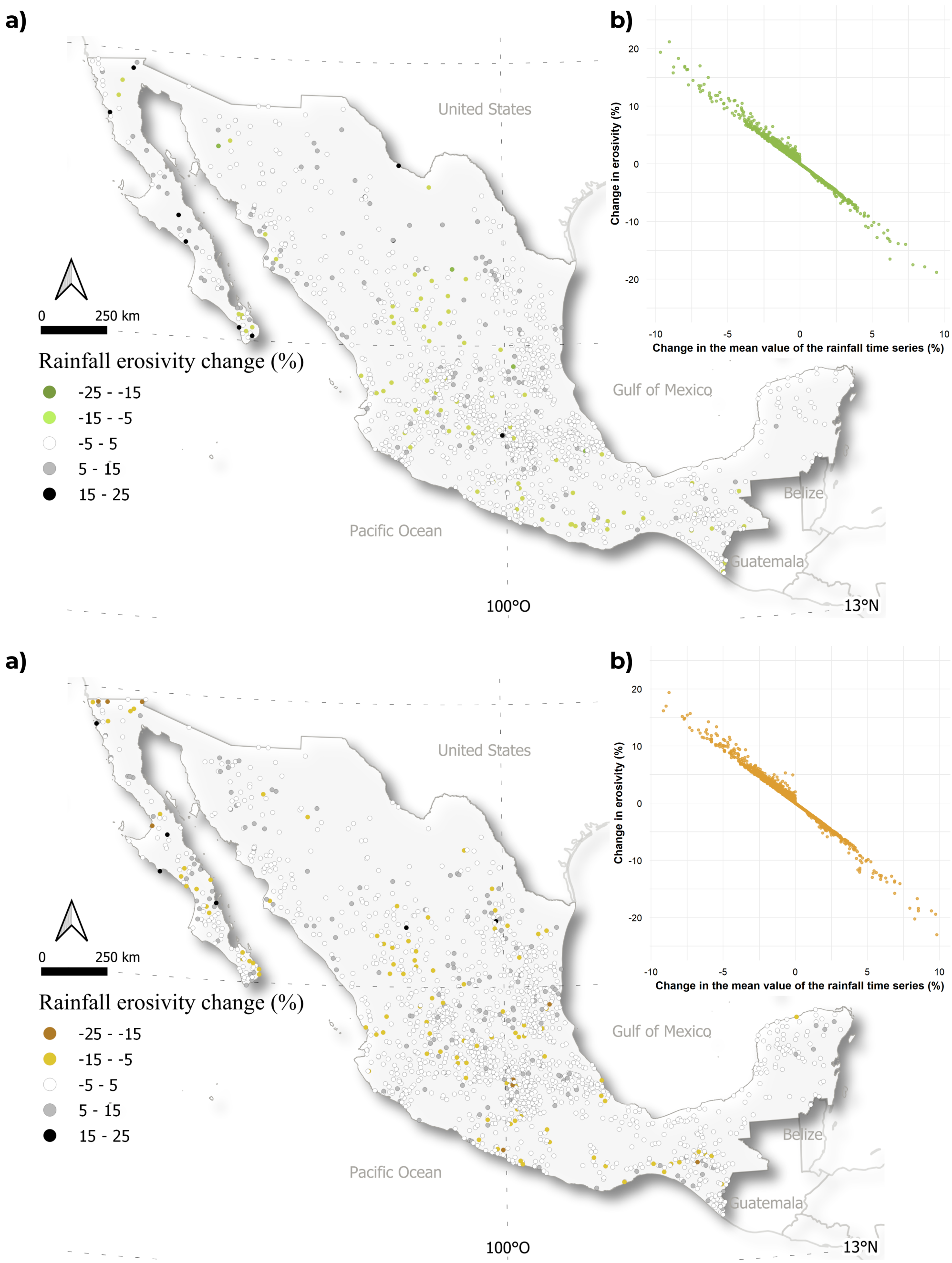

Figure A6. Percentage changes in rainfall erosivity after modifying precipitation time series according to the percentage change in the mean value of the rainfall time series before and after the gap-filling and homogenization processes. Upper panel: climate normal 1968–1997. Bottom panel: climate normal 1978–2007. a) Spatial distribution of percentage changes in rainfall erosivity. b) Relationship between percentage changes in the mean value of the rainfall time series and percentage changes in rainfall erosivity.

Table A5. Mean rainfall erosivity and mean percentage change in erosivity by ecoregion for the three climate normals. Percentage changes were estimated from modifications to the rainfall time series resulting from the gap-filling and homogenization processes. Eco: Ecoregion (1: Mediterranean California, 2: North American Deserts, 3: Semi-arid Elevations, 4: Great Plains, 5: Tropical Rain Forest, 6: Tropical Dry Forest, 7: Temperate Sierras)

Climate Normal	Eco	Mean erosivity (MJ mm ha^{-1} h^{-1} yr^{-1})	Mean change (MJ mm ha^{-1} h^{-1} yr^{-1})	Mean change (%)	Minimum change (%)	Maximum change (%)
1968-1997	1	562	6.0	2.1	-4.6	16.9
	2	1133	16.0	2.3	-17.9	21.2
	3	2072	9.6	0.5	-13.1	12.4
	4	4349	54.5	1.4	-2.1	6.5
	5	14033	8.1	0.3	-11.5	6.5
	6	5627	26.3	0.6	-14.0	16.8
	7	4743	9.7	0.5	-18.8	17.0
1978-2007	1	541	-0.1	0.7	-20.3	17.0
	2	1122	20.1	1.7	-18.9	19.3
	3	2020	8.9	0.3	-13.3	12.5
	4	4240	-23.0	-0.6	-13.8	8.8
	5	12755	78.7	0.6	-10.3	11.2
	6	5628	23.1	0.4	-19.5	13.2
	7	4075	15.8	0.7	-23.0	15.2
1988-2017	2	1455	-2.8	-0.4	-18.7	17.2
	3	2134	13.1	0.3	-16.3	13.0
	4	4184	-6.9	-0.4	-17.6	9.7
	5	12019	26.4	0.1	-6.7	16.6
	6	5942	60.9	0.7	-16.9	17.6
	7	4566	36.5	0.6	-19.3	16.2

Appendix B: Description of the methods and materials used by Cortés (1991)

This supplementary material presents translated excerpts from the Materials and Methods section of the master's thesis by Cortés (1991), Caracterización de la erosividad de la lluvia en México utilizando métodos multivariados, developed at the Colegio de Posgraduados (Montecillo, Mexico) in 1991. These excerpts describe the procedures used to construct the rainfall erosivity dataset employed in this study as a validation dataset. Because the original thesis is only available in physical format and written in Spanish, the most relevant sections were translated into English to facilitate understanding and reproducibility for non-Spanish-speaking readers. The translated material includes the procedures for pluviogram reading, rainfall event definition, and calculation of rainfall intensities and the EI30 index. A physical copy of the thesis is available at the Colegio de Posgraduados library, and the catalog information can be accessed at (http://catalogo.colpos.mx/cgi-bin/koha/opac-detail.pl?biblionumber=17230). A complete scanned PDF version of the original thesis is available from the authors upon request.

-Pages 11, 12 and 13

III. LITERATURE REVIEW

3.3.2.1. Wischmeier Index $(EI30)$

The $EI30$ index was proposed by Wischmeier (1959) and is defined as the product of the total kinetic energy of rainfall (E) and the maximum 30-minute intensity $(I30)$. It measures the effect in which erosion caused by splash detachment and flow turbulence combine with runoff to remove detached soil particles from the land surface. This process is known as sheet erosion. Its calculation is performed using the following equation:

$EI30 = (E)(I30)$

where $EI30$ is the erosivity index for a rainfall event (MJ mm ha^{-1} h^{-1}). E is the total kinetic energy of rainfall (MJ ha^{-1}). $I30$ is the maximum rainfall intensity in 30 minutes (mm h^{-1}).

The kinetic energy of rainfall is obtained using the equation:

$E = \sum_{j=1}^{n} e_j P_j$

where e_j is the kinetic energy for the time interval j (MJ ha^{-1} mm^{-1}). P_j is the amount of rainfall during the time interval j (mm). n is the number of intervals with different intensity during the same event.

The calculation of e_j in units of the International System is carried out using the equation (Wischmeier and Smith, 1978; Foster et al., 1981):

$e_j = 0.119 + 0.0873 \log_{10} I_j; \quad I_j \leq 76 \text{ mm hr}^{-1}$

$e_j = 0.283; \quad I_j > 76 \text{ mm hr}^{-1}$

where I_j is the rainfall intensity during interval j (mm h^{-1}); $I_j = \frac{P_j(60)}{t_j}$, t_j is the duration of interval j (minutes) and e_j and P_j were already defined.

The multiplication by (60) converts the data into hourly units. The value of e_j becomes constant for $I > 76$ mm h^{-1} because it is considered that, at higher intensities, the size of raindrops no longer increases (Wischmeier and Smith, 1978).

The sum of the $EI30$ values during one year forms the annual rainfall erosivity factor (R) of the Universal Soil Loss Equation (USLE), proposed by Wischmeier and Smith (1978) and expressed as:

$A = RKLSCP$

where A is the average annual soil loss (Ton ha^{-1}), R is the rainfall erosivity factor (MJ ha^{-1} h^{-1}), K is the soil erodibility factor (Ton ha h MJ^{-1} mm^{-1} ha^{-1}), L is the slope length factor (dimensionless), S is the slope steepness factor (dimensionless), C is the crop management factor (dimensionless), and P is the support practice factor for erosion control (dimensionless)

The algebraic expression of R is therefore:

$R = \sum_{i=1}^{m} (EI30)_i$

where R is the rainfall erosivity factor or annual erosivity index (MJ mm ha^{-1} h^{-1} yr^{-1}) and m is the number of rainfall events during the year.

The $EI30$ has proven to be an efficient rainfall erosivity index for estimating soil loss in different parts of the world, although originally developed for the region east of the Rocky Mountains in the United States. In other cases, however, (Lal, 1979; Roose, 1979; Hudson, 1981), the correlations between $EI30$ and soil loss have been low, and better results have been found when considering other approaches, thus obtaining other erosivity indices.

-Pages 40, 43, 44 and 45

IV. MATERIALS AND METHODS

4.1 Materials

The materials used were: daily-recording pluviograms, digitizing tablets, microcomputers, and floppy disks for microcomputers. The statistical analysis of the information was carried out using the SAS, STATGRAPHICS, and GEOEAS statistical packages. The latter, perhaps less widely known than the previous two, is a geostatistical package (Geostatistical Environmental Assessment Software: GEOEAS) developed by the U.S. EPA Environmental Monitoring Systems Laboratory in Las Vegas, Nevada, in cooperation with the Department of Applied Earth Sciences at Stanford University. It is useful for interpolation studies because, in addition to allowing the calculation of basic statistics and scatterplots of variables, it generates variograms for one or more variables in bidimensional space, enables validation of such variograms, and based on them, kriging can be performed (estimating values for a grid of points). It also has the capability to generate contour maps of isovalues for the variable of interest. Harvard Graphics was also used in the preparation of some figures and graphs. The programs used for data acquisition and information processing were written in BASIC and PASCAL programming languages.

4.2 Methodology

4.2.1 Data acquisition, organization, and classification

The development of the present work was based on the analysis of pluviograms provided by the National Meteorological Service (SMN). The number and names of the stations are presented in Table 4.2.1, and their location can be seen in Figure 4.2.1.

The selection of stations was based on the assumption that a greater number of years analyzed would produce more reliable results, as shown by the experience of studies conducted in different parts of the world related to rainfall erosivity. Thus, it was found that although there is no number of years defined as a minimum, there is consensus (Stocking and Elwell, 1976; Moldenhauer, 1980) that a period equal to or greater than 20 years would be desirable.

Finally, the determining factor appears to be data availability, and as expected, developing countries generally do not have the same number and equipment of meteorological stations available in more developed countries. While Koolhaas (1977) presents an isoerodent map (lines connecting points with equal mean annual rainfall erosivity) for Uruguay based on the analysis of pluviograms from a single meteorological station (and estimated values for another 100 stations using a regression equation), the isoerodent map for the United States (Koolhaas, 1977) was obtained from the analysis of 181 pluviographs (estimating values for another 1700 locations using a regression equation).

Based on the above, and also considering that the work to be carried out is laborious, it was decided to analyze an uninterrupted 11-year period of rainfall data from 1977 to 1987, inclusive. However, the number of stations in Mexico meeting this requirement is quite limited (approximately 20 were found within the SMN), and their spatial distribution across the national territory is deficient. Consequently, it was necessary to make considerations regarding the minimum number of years of available information (pluviograms) that each station should fulfill. Therefore, it was decided to accept 51 stations that had a minimum of four consecutive years of data records. Finally, the Ceicades-CP station (53) in Cárdenas, Tabasco, with only one year of information, and Ocozocuatla, Chiapas (52), with six non-consecutive years of information, were included because the sample coverage in that area was very poor and it was desirable to have some reference data for the region. It was also found that the stations of Santa Rosalía, Baja California Sur; Cuernavaca, Morelos; Puerto Ángel, Oaxaca; and Tapachula, Chiapas, did not strictly meet the aforementioned restrictions, since they lacked one month of data (Cuernavaca lacked two months) within the four-year historical period. Nevertheless, despite the above, these stations were also included in the analysis.

In total, information from 53 meteorological stations was used. Table A.1 in the Appendix presents the years analyzed for each station.

4.2.2. Reading of pluviograms

For the reading of pluviograms, all rainfall events were considered, regardless of how small the precipitation depth was; therefore, every event recorded by the pluviograph was taken into account in the study.

To perform the reading process, the PLUVIOGRAMAS program in Applesoft BASIC for the Apple II microcomputer was used. In combination with a digitizing tablet, the program allowed the coordinates of the pluviograph chart to be read and subsequently performed the required calculations (the program can be consulted in the work of Cortés, 1987).

To define an individual rainfall event or storm, the criterion proposed by Wischmeier (1959) was followed. In developing the EI30 erosivity index, he found better results when a rainfall event was considered independent from another only if there was a rainless interval of 6 or more hours between them.

4.2.3. Procedure for calculating maximum rainfall intensities and erosivity indices

The calculation of maximum rainfall intensities for different duration periods (5, 10, 15, 30, 45, 60, 90, and 120 minutes) and erosivity indices was performed using the previously mentioned PLUVIOGRAMAS program. The procedure used to determine maximum rainfall intensities is presented below.

The different intensities within a particular rainfall event were determined using the time (t) and rainfall depth (h) coordinates at the points where the slope of the curve traced by the pluviograph changed. Using these intensities (I), an array was generated to obtain the maximum intensities for durations of 5, 10, 15, 30, 45, 60, 90, and 120 minutes. The calculation is described by the following algorithm.

The maximum intensity $(Imax)$ for a duration of T_i minutes is:
$Imax_{T_i} = \frac{1}{T_i}\left[\sum_{i=1}^{n-1}(I_i d_i) + I_n\left(T_i - \sum_{i=1}^{n-1} d_i\right)\right]$

Where i is the position of the intensities (I) selected together with their respective duration (d). Example: $i = 1$ is assigned to the highest intensity, $i = 2$ to the second highest intensity, and so on in descending order of magnitude, searching above and below the highest intensity. n is the position of the last intensity that must be selected because its respective duration added to the previous one exceeds T_i (or is equal to T_i). Thus, the duration taken from this last intensity is the number of minutes necessary to complete T_i.

For the calculation of erosivity indices, the corresponding equations are incorporated into the program, as described in Section 3.3.2 of the Literature Review. The indices are calculated for each storm event; therefore, by summing the values occurring within a month, the monthly value is obtained; if all the values for a year are summed, the annual value is obtained.

Table B1: Average annual rainfall depth values and $EI30$ values for 54 meteorological stations used by Cortés (1991). This table is named as "Cuadro 5.1.2" in the original master thesis of Cortés (1991)

WS Name	WS Code	Latitude	Longitude	Altitude (m)	Rainfall (mm)	EI30	Years
Sta Rosalia	1	27.283	112.317	75	130.3	226.2	3
Loreto	2	26.017	111.350	15	155.7	504	8
Constitución	3	24.950	111.700	48	125	536	5
La Paz	4	24.083	110.333	17	204.6	820.8	9
Hermosillo	5	29.067	110.967	211	244.9	2791.8	11
Empalme	6	27.983	110.767	11	184.2	936.8	6
Cd. Obregón	7	27.483	109.933	38	307.1	1409.9	11
Choix	8	26.717	108.333	238	780	3025.4	5
Culiacan	9	24.800	107.400	39	630.4	3366.4	6
Mazatlan	10	23.217	106.417	2	800.3	6371.9	5
Tepehuanes	11	25.350	105.750	1967	484.1	978.8	4
Torreon	12	25.533	103.450	1124	217.1	1136.7	11
Monclova	13	26.883	101.433	615	338.4	1730.1	5
Saltillo	14	25.417	100.983	1609	303.9	1440.7	66
Monterrey	15	25.683	100.300	512	634.1	2235.1	66
Soto La Marina	16	23.767	98.217	21	751.8	3595	5
Tepic	17	21.517	104.900	922	1348	6329.3	11

Table B1 continued from previous page

WS Name	WS Code	Latitude	Longitude	Altitude (m)	Rainfall (mm)	EI30	Years
Manzanillo	18	19.050	104.317	3	1070.7	6152.1	11
Colotlan	19	22.117	103.267	1673	660.5	2027.3	10
Lagos de M.	20	21.350	101.917	1880	558.2	2004.3	10
Guadalajara	21	20.683	103.383	1551	902.3	5887.2	10
Cd. Guzman	22	19.700	103.467	1507	731.6	3284	7
P.El chique	23	22.000	102.900	1514	554.1	1772.5	6
Ceuvag	24	24.417	104.317	1951	486.1	953.2	6
Aguascalientes	25	21.867	102.300	1874	535	1372.6	7
San Luis de Potosí	26	22.150	100.983	1877	359.4	1232.8	11
Rio verde	27	21.933	99.983	990	497	1599.4	11
Matlapa	28	21.333	98.800	133	1938.6	16551.5	9
Tulancingo	29	20.083	98.367	2181	552.9	908.9	11
Pachuca	30	20.133	98.733	2417	386.8	700.9	11
Leon	31	21.100	101.683	1850	619.8	1526.6	4
Guanajuato	32	21.017	101.250	1999	683.7	2401.5	7
Morelia	33	19.700	101.183	1912	760.7	2048	10
Toluca	34	19.283	99.667	2720	800.2	1936.1	10
Tacubaya	35	19.400	99.200	2308	720.8	3628.3	11
Cuernavaca	36	18.917	99.233	1560	1061	5959.7	3
Puebla	37	19.033	98.183	2162	822.9	3909.7	11
Tlaxcala	38	19.317	98.233	2252	802.3	3430.2	9
Tuxpan	39	20.950	97.400	28	1350.9	5011.8	8
Jalapa	40	19.533	96.917	1389	1514.8	4846.9	6
Orizaba	41	18.850	97.100	1259	235.51	11917.2	10
Veracruz	42	19.200	96.133	2	1667.6	12411.1	9
Coatzacoalcos	43	18.133	94.417	22	2726.2	25653.9	10
Chilpancingo	44	17.550	99.500	1360	820.7	1654.7	11
Acapulco	45	16.750	99.767	3	1412.2	6758.3	8
Puerto Angel	46	15.683	96.483	46	1038.9	8531.1	2
Huajuapan Dl.	47	17.800	97.767	1650	720.5	2126.8	9
Tuxctla gtz.	48	16.750	93.117	536	948.2	8639.4	5
Tapachula	49	14.917	92.267	117	2488.9	25249.1	3
Mérida	50	20.933	89.633	9	940	7680.2	10

Table B1 continued from previous page

WS Name	WS Code	Latitude	Longitude	Altitude (m)	Rainfall (mm)	EI30	Years
Valladolid	51	20.683	88.217	18	1158.8	10865.1	8
Ocozocuatla	52	16.767	93.383	864	897.5	2114.6	4
Ceicades-CP	53	18.017	93.383	23	2240.3	6499	1

Author contributions. VMVR, DAGL, and MG contributed with conceptualization, formal analysis, Methodology, and visualization. VMVR, DAGL, and CEAC contributed to the data curation and writing - original draft preparation. CEAC, AGT, BLPP, DLL, RRGLL, and MG contributed to Project administration, writing, review, and editing. VMVR, BLPP, and MG contributed to funding acquisition.

Competing interests. The authors declare that they have no conflict of interest.

Acknowledgements. VMVR and CEAC acknowledged support from SECIHTI scholarship (PhD level,CVU: 1240028, 1268803, respectively). VMVR, BLPP, and MG acknowledge support from grant CF-2023-I-1846 of the National Council of Humanities, Sciences, and Technologies; abbreviated CONAHCYT. VMVR acknowledges the Corporación Colombiana de Investigación Agropecuaria (AGROSAVIA) for granting a study leave. Authors acknowledge support from grant IGCP-765 and from UNAM PAPIIT IG101325. The authors want to thank to the National Meteorological Service (SMN by its initials in Spanish) and National Water Commission (CONAGUA by its initials in Spanish) for making public available the national climate data.

References

Abbruzzini, T. F., Figueroa, D., Cruz, C. E. A., Varón-Ramírez, V. M., Santamaria, M. A. G., and Prado, B.: Assessing soil nutrient spatial variability in Mexico through digital soil mapping: Implications for sustainable agriculture, Geoderma Regional, 45, e01 081, https://doi.org/https://doi.org/10.1016/j.geodrs.2026.e01081, 2026.

Adeyeri, O., Lamptey, B., Lawin, A., and Sanda, I.: Spatio-Temporal Precipitation Trend and Homogeneity Analysis in Komadugu-Yobe Basin, Lake Chad Region, Journal of Climatology Weather Forecasting, 5, https://doi.org/10.4172/2332-2594.1000214, 2017.

Adeyeri, O., Laux, P., Ishola, K., Zhou, W., Balogun, I., Adeyewa, Z., and Kunstmann, H.: Homogenising meteorological variables: Impact on trends and associated climate indices, Journal of Hydrology, 607, 127 585, https://doi.org/https://doi.org/10.1016/j.jhydrol.2022.127585, 2022.

Agustín Breña-Naranjo, J., Pedrozo-Acuña, A., Pozos-Estrada, O., Jiménez-López, S. A., and López-López, M. R.: The contribution of tropical cyclones to rainfall in Mexico, Physics and Chemistry of the Earth, Parts A/B/C, 83-84, 111–122, https://doi.org/https://doi.org/10.1016/j.pce.2015.05.011, emerging science and applications with microwave remote sensing data, 2015.

Alexandersson, H.: A homogeneity test applied to precipitation data, Journal of Climatology, 6, 661–675, https://doi.org/https://doi.org/10.1002/joc.3370060607, 1986.

Almagro, A., Oliveira, P. T. S., Nearing, M. A., and Hagemann, S.: Projected climate change impacts in rainfall erosivity over Brazil, Scientific Reports, 7, 8130, https://doi.org/10.1038/s41598-017-08298-y, 2017.

Beck, H. E., Zimmermann, N. E., McVicar, T. R., Vergopolan, N., Berg, A., and Wood, E. F.: Present and future Köppen-Geiger climate classification maps at 1-km resolution, Scientific Data, 5, 180 214, https://doi.org/10.1038/sdata.2018.214, 2018.

Benites, E. T., Becerra, J. C., Gil, J. U., Cedillo, L. T., and Torres, P. S. R.: Predicción de la erosión hídrica en la cuenca del Cañón del Sumidero, Chiapas, Revista Mexicana de Ciencias Agrícolas, 11, 1903–1915, https://doi.org/10.29312/remexca.v11i8.2747, epub 13 de diciembre de 2021, 2020.

Bezak, N., Borrelli, P., and Panagos, P.: Exploring the possible role of satellite-based rainfall data in estimating inter- and intra-annual global rainfall erosivity, Hydrology and Earth System Sciences, 26, 1907 – 1924, https://doi.org/10.5194/hess-26-1907-2022, cited by: 26; All Open Access, Gold Open Access, Green Open Access, 2022.

Bolaños González, M. A., Paz Pellat, F., Cruz Gaistardo, C. O., Argumedo Espinoza, J. A., Romero Benítez, V. M., and de la Cruz Cabrera, J. C.: Mapa de erosión de los suelos de México y posibles implicaciones en el almacenamiento de carbono orgánico del suelo, Terra Latinoamericana, 34, 271–288, http://www.scielo.org.mx/scielo.php?script=sci_arttext&pid=S0187-57792016000300271&lng=es&tlng=es, recuperado en 03 de septiembre de 2024, 2016.

Boos, W. R. and Pascale, S.: Mechanical forcing of the North American monsoon by orography, Nature, 599, 611 – 615, https://doi.org/10.1038/s41586-021-03978-2, all Open Access, Green Open Access, 2021.

Borrelli, P., Robinson, D., Fleischer, L. R., Lugato, E., Ballabio, C., Alewell, C., Meusburger, M., Modugno, P., Schütt, M., Tenuta, K. E., and Panagos, P.: Land use and climate change impacts on global soil erosion by water (2015-2070), Proceedings of the National Academy of Sciences, 117, 21 994–22 001, https://doi.org/10.1073/pnas.2001403117, 2020.

Borrelli, P., Ballabio, C., Yang, J. E., Robinson, D. A., and Panagos, P.: GloSEM: High-resolution global estimates of present and future soil displacement in croplands by water erosion, Scientific Data, 9, 406, https://doi.org/10.1038/s41597-022-01489-x, 2022.

Cardoso, D. P., Silva, E. M., Avanzi, J. C., Muniz, J. A., Ferreira, D. F., Silva, M. L. N., Acuña-Guzman, S. F., and Curi, N.: RainfallErosivityFactor: An R package for rainfall erosivity (R-factor) determination, CATENA, 189, 104 509, https://doi.org/https://doi.org/10.1016/j.catena.2020.104509, 2020.

Carrera, J. J., Levresse, G. P., and Hernández-Espriú, J. A.: Geostatistical Analysis of Yearly Precipitation at the National Level: Stratification and Anisotropy Considerations in Mexico, pre-print available at SSRN: https://ssrn.com/abstract=4820011 or http://dx.doi.org/10.2139/ssrn.4820011, 2024.

Carrera-Hernández, J. J.: Mexico's High Resolution Climate Database (MexHiResClimDB): a new daily high-resolution gridded climate dataset for Mexico covering 1951–2020, Earth System Science Data Discussions, 2025, 1–30, https://doi.org/10.5194/essd-2025-100, 2025.

Chen, Y., Xu, M., Wang, Z., Chen, W., and Lai, C.: Reexamination of the Xie model and spatiotemporal variability in rainfall erosivity in mainland China from 1960 to 2018, CATENA, 195, 104 837, https://doi.org/https://doi.org/10.1016/j.catena.2020.104837, 2020.

Commission for Environmental Cooperation: Ecological Regions of North America -Toward a Common Perspective, Commission for Environmental Cooperation, Montreal, Canada, ISBN 2-922305-20-1, 1997.

Cortés, H. G.: Caracterización de la erosividad de la lluvia en México utilizando métodos multivariados, Master's thesis, Colegio de Posgraduados, Montecillo, Mexico, centro de Edafología, 1991.

Cuervo-Robayo, A. P., Téllez-Valdés, O., Gómez-Albores, M. A., Venegas-Barrera, C. S., Manjarrez, J., and Martínez-Meyer, E.: An update of high-resolution monthly climate surfaces for Mexico, International Journal of Climatology, 34, 2427 – 2437, https://doi.org/10.1002/joc.3848, cited by: 153, 2014.

Cuervo-Robayo, A. P., Ureta, C., Gómez-Albores, M. A., Meneses-Mosquera, A. K., Téllez-Valdés, O., and Martínez-Meyer, E.: One hundred years of climate change in Mexico, PLOS ONE, 15, 1–19, https://doi.org/10.1371/journal.pone.0209808, 2020.

Das, S., Jain, M. K., Gupta, V., McGehee, R. P., Yin, S., de Mello, C. R., Azari, M., Borrelli, P., and Panagos, P.: GloRESatE: A dataset for global rainfall erosivity derived from multi-source data, Scientific Data, 11, 926, https://doi.org/10.1038/s41597-024-03756-5, 2024.

Dawoud, O., Eljamassi, A., and Abunada, Z.: Mapping and Quantification of Soil Erosion and Sediment Delivery in Poorly Developed Urban Areas: A Case Study, Sustainability, 15, https://doi.org/10.3390/su151813683, 2023.

de Anda Sánchez, J.: Precipitation in Mexico, pp. 1–14, Springer International Publishing, Cham, ISBN 978-3-030-40686-8, https://doi.org/10.1007/978-3-030-40686-8_1, 2020.

Deitch, M. J., Sapundjieff, M. J., and Feirer, S. T.: Characterizing Precipitation Variability and Trends in the World's Mediterranean-Climate Areas, Water, 9, https://doi.org/10.3390/w9040259, 2017.

Dunkerley, D. L.: Rainfall intensity bursts and the erosion of soils: an analysis highlighting the need for high temporal resolution rainfall data for research under current and future climates, Earth Surface Dynamics, 7, 345–360, https://doi.org/10.5194/esurf-7-345-2019, 2019.

Duwal, S., Prajapati, R., Upadhyay, S., Neupane, S., Lakhe, H., Thapa, B. R., Davids, J. C., and Talchabhadel, R.: Leveraging a Citizen Science Approach for Rainfall Monitoring: Evaluating Performance and Reliability To Complement Standard Datasets, Earth Systems and Environment, https://doi.org/10.1007/s41748-025-00920-8, 2025.

Efthimiou, N.: Evaluating the performance of different empirical rainfall erosivity (R) factor formulas using sediment yield measurements, CATENA, 169, 195–208, https://doi.org/https://doi.org/10.1016/j.catena.2018.05.037, 2018.

Feng, Z., Zhang, Z., Zuo, Y., Wan, X., Wang, L., Chen, H., Xiong, G., Liu, Y., Tang, Q., and Liang, T.: Analysis of long term water quality variations driven by multiple factors in a typical basin of Beijing-Tianjin-Hebei region combined with neural networks, Journal of Cleaner Production, 382, 135 367, https://doi.org/https://doi.org/10.1016/j.jclepro.2022.135367, 2023.

Fenta, A. A., Tsunekawa, A., Haregeweyn, N., Yasuda, H., Tsubo, M., Borrelli, P., Kawai, T., Sewale Belay, A., Ebabu, K., Liyew Berihun, M., Sultan, D., Asamin Setargie, T., Elnashar, A., and Panagos, P.: Improving satellite-based global rainfall erosivity estimates through merging with gauge data, Journal of Hydrology, 620, https://doi.org/10.1016/j.jhydrol.2023.129555, cited by: 15; All Open Access, Hybrid Gold Open Access, 2023.

Fransiska, H., Agustina, D., Setyorini, D., Sumartajaya, I. M., and Kurnia, A.: Time Series Clustering Analysis Using Dynamic Time Warping Technique of Daily Rainfall in Bengkulu Province, IOP Conference Series: Earth and Environmental Science, 1359, 012 026, https://doi.org/10.1088/1755-1315/1359/1/012026, 2024.

García, E.: Climas (clasificación de Köppen, modificado por García), Map, scale 1:1,000,000, méxico, 1998.

Gochis, D. J., Brito-Castillo, L., and Shuttleworth, W. J.: Hydroclimatology of the North American Monsoon region in northwest Mexico, Journal of Hydrology, 316, 53–70, https://doi.org/https://doi.org/10.1016/j.jhydrol.2005.04.021, 2006.

González, O. N., Serrano, J. I. B., Vílchez, F. F., Núñez, R. M. M., and García-Sancho, A. G.: Riesgo de erosión hídrica y estimación de pérdida de suelo en paisajes geomorfológicos volcánicos en México, Cultivos Tropicales, 37, 45–55, http://scielo.sld.cu/scielo.php?script=sci_arttext&pid=S0258-59362016000200006&lng=es&tlng=es, recuperado en 02 de septiembre de 2024, 2016.

Guerrero, E., Pérez, A., Arroyo, C., Equihua, J., and Guevara, M.: Building a National Framework for Pedometric Mapping: Soil Depth as an Example From Mexico, in: GlobalSoilMap, edited by Arrouays, D., McKenzie, N., Hempel, J., Forges, A., and McBratney, A., pp. 103–108, CRC Press, ISBN 978-1-138-00119-0, 2014.

Guijarro, J. A.: Quality control and homogenization of climatological series, https://doi.org/10.1201/b15625, cited by: 5, 2014.

Guijarro, J. A.: climatol: Climate Tools (Series Homogenization and Derived Products), https://CRAN.R-project.org/package=climatol, r package version 4.1.0, 2024.

Guo, C., Chen, Y., Xia, W., Qu, X., Yuan, H., Xie, S., and Lin, L.-S.: Eutrophication and heavy metal pollution patterns in the water suppling lakes of China's south-to-north water diversion project, Science of The Total Environment, 711, 134 543, https://doi.org/https://doi.org/10.1016/j.scitotenv.2019.134543, 2020.

Gómez-Latorre, D. A., Araujo-Carrillo, G. A., and Leguizamón, Y. R.: Regionalización de patrones de lluvias para períodos multianuales secos y húmedos en el Altiplano Cundiboyacense de Colombia, Revista de Climatología, 22, 162–177, https://rclimatol.eu/2022/12/31/regionalizacion-de-patrones-de-lluvias-para-periodos-multianuales-secos-y-humedos-en-el-altiplano-cundiboyacense-de-colombia/, 2022.

Hanel, M., Máca, P., Bašta, P., Vlnas, R., and Pech, P.: The rainfall erosivity factor in the Czech Republic and its uncertainty, Hydrology and Earth System Sciences, 20, 4307–4322, https://doi.org/10.5194/hess-20-4307-2016, 2016.

Hartigan, J. A.: Clustering algorithms, John Wiley & Sons, Inc., 1975.

Hatfield, J. L., Sauer, T. J., and Cruse, R. M.: Chapter One - Soil: The Forgotten Piece of the Water, Food, Energy Nexus, Advances in Agronomy, 143, 1–46, https://doi.org/https://doi.org/10.1016/bs.agron.2017.02.001, 2017.

INEGI-CONABIO-INE: Ecorregiones Terrestres de México, Tech. rep., Instituto Nacional de Estadística, Geografía e Informática (INEGI) and Comisión Nacional para el Conocimiento y Uso de la Biodiversidad (CONABIO) and Instituto Nacional de Ecología (INE), México, escala 1:1000000, 2008.

Jiménez Espinosa, M., Baeza Ramírez, C., Matías Ramírez, L. G., and Eslava Morales, H.: Mapas de Índices de Riesgo a Escala Municipal por Fenómenos Hidrometeorológicos, Informe técnico, Sistema Nacional de Protección Civil, Centro Nacional de Prevención de Desastres (CENAPRED), México, http://www.atlasnacionalderiesgos.gob.mx/descargas/Metodologias/Hidrometeorologico.pdf, subdirección de Riesgos Hidrometeorológicos, 2012.

Karami, A., Homaee, M., Neyshabouri, M. R., Afzalinia, S., and Basirat, S.: Large scale evaluation of single storm and short/long term erosivity index models, Turkish Journal of Agriculture and Forestry, 36, 207 – 216, https://doi.org/10.3906/tar-1102-24, cited by: 9; All Open Access, Bronze Open Access, 2012.

Kim, J., Han, H., Kim, B., Chen, H., and Lee, J.-H.: Use of a high-resolution-satellite-based precipitation product in mapping continental-scale rainfall erosivity: A case study of the United States, CATENA, 193, 104 602, https://doi.org/https://doi.org/10.1016/j.catena.2020.104602, 2020.

Kumar, M., Sahu, A. P., Sahoo, N., Nayak, A. K., Tinde, L. K., Panda, M. R., Palmate, S., and Dash, S. S.: A Global Review of Rainfall Erosivity Estimation: Methods, Challenges, and Way Forward, Earth Systems and Environment, https://doi.org/10.1007/s41748-025-01006-1, 2026.

Li, J., Sun, R., and Chen, L.: Assessing the accuracy of large-scale rainfall erosivity estimation based on climate zones and rainfall patterns, CATENA, 217, 106 508, https://doi.org/https://doi.org/10.1016/j.catena.2022.106508, 2022.

Liu, Y., Zhao, W., Liu, Y., and Pereira, P.: Global rainfall erosivity changes between 1980 and 2017 based on an erosivity model using daily precipitation data, CATENA, 194, 104 768, https://doi.org/https://doi.org/10.1016/j.catena.2020.104768, 2020.

Lobo, G. P. and Bonilla, C. A.: Effect of temporal resolution on rainfall erosivity estimates in zones of precipitation caused by frontal systems, CATENA, 135, 202–207, https://doi.org/https://doi.org/10.1016/j.catena.2015.08.002, 2015.

Matthews, F., Borrelli, P., Panagos, P., and Bezak, N.: Dynamic assessment of rainfall erosivity in Europe: evaluation of EURADCLIM ground-radar data, Hydrology and Earth System Sciences, 29, 5299–5313, https://doi.org/10.5194/hess-29-5299-2025, 2025.

McCuen, R. H.: Hydrologic Analysis and Design, Pearson, 4th edition edn., ISBN 978-0134313122, 2016.

Meng, X., Zhu, Y., Yin, M., and Liu, D.: The impact of land use and rainfall patterns on the soil loss of the hillslope, Scientific Reports, 11, 16 341, https://doi.org/10.1038/s41598-021-95819-5, 2021.

Min, K., Yang, Y., Wahab, L., Woo, S., Oh, M., Ghezzehei, T. A., and Asefaw Berhe, A.: Soil organic matter dynamics under changing precipitation regimes, New Phytologist, 249, 2179–2195, https://doi.org/https://doi.org/10.1111/nph.70804, 2026.

Nearing, M. A.: Soil Erosion and Conservation, p. Chapter page numbers if available, Wiley, 2nd edn., https://digitalcommons.unl.edu/usdaarsfacpub/1290/, 2013.

Nearing, M. A., qing Yin, S., Borrelli, P., and Polyakov, V. O.: Rainfall erosivity: An historical review, CATENA, 157, 357–362, https://doi.org/https://doi.org/10.1016/j.catena.2017.06.004, 2017.

Panagos, P., Borrelli, P., Meusburger, K., Yu, B., Klik, A., Jae Lim, K., Yang, J. E., Ni, J., Miao, C., Chattopadhyay, N., Sadeghi, S. H., Hazbavi, Z., Zabihi, M., Larionov, G. A., Krasnov, S. F., Gorobets, A. V., Levi, Y., Erpul, G., Birkel, C., Hoyos, N., Naipal, V., Oliveira, P. T. S., Bonilla, C. A., Meddi, M., Nel, W., Al Dashti, H., Boni, M., Diodato, N., Van Oost, K., Nearing, M., and Ballabio, C.: Global rainfall erosivity assessment based on high-temporal resolution rainfall records, Scientific Reports, 7, 4175, https://doi.org/10.1038/s41598-017-04282-8, 2017.

Panagos, P., Hengl, T., Wheeler, I., Marcinkowski, P., Rukeza, M. B., Yu, B., Yang, J. E., Miao, C., Chattopadhyay, N., Sadeghi, S. H., Levi, Y., Erpul, G., Birkel, C., Hoyos, N., Oliveira, P. T. S., Bonilla, C. A., Nel, W., Al Dashti, H., Bezak, N., Van Oost, K., Petan, S., Fenta, A. A., Haregeweyn, N., Pérez-Bidegain, M., Liakos, L., Ballabio, C., and Borrelli, P.: Global rainfall erosivity database (GloREDa) and monthly R-factor data at 1 km spatial resolution, Data in Brief, 50, 109 482, https://doi.org/https://doi.org/10.1016/j.dib.2023.109482, 2023.

Paulhus, J. L. H. and Kohler, M. A.: Interpolation of missing precipitation records, Monthly Weather Review, 80, 129–133, https://doi.org/10.1175/1520-0493(1952)080<0129:IOMPR>2.0.CO;2, 1952.

Pennock, D.: Soil erosion: the greatest challenge for sustainable soil management, FAO, Rome, Italy, ISBN 978-92-5-131426-5, https://openknowledge.fao.org/items/6c070e1e-6533-4b7e-ba5f-a2f21a0e59ff, 2019.

Pianosi, F., Beven, K., Freer, J., Hall, J. W., Rougier, J., Stephenson, D. B., and Wagener, T.: Sensitivity analysis of environmental models: A systematic review with practical workflow, Environmental Modelling Software, 79, 214–232, https://doi.org/https://doi.org/10.1016/j.envsoft.2016.02.008, 2016.

Porrúa, F. E., Hidalgo, J. Z., Arroyo, A. M., Raga, G., and García, C. G.: Estado y perspectivas del Cambio Climático en México: un punto de partida, Tech. rep., Universidad Nacional Autónoma de México, Mexico, ISBN 978-607-30-8172-6, https://cambioclimatico.unam.mx/estado-y-perspectivas-del-cambio-climatico-en-mexico/, 2020.

Qiao, Z., Ma, L., Xu, Y., Yang, D., Liu, T., and Chen, Y.: Future climate change impacts on carbon dynamics and ecohydrological risks in the West Liao river Basin, China: implications for carbon management, Carbon Balance and Management, 21, 8, https://doi.org/10.1186/s13021-025-00339-8, 2025.

Renard, K. G. and Freimund, J. R.: Using monthly precipitation data to estimate the R-factor in the revised USLE, Journal of Hydrology, 157, 287–306, https://api.semanticscholar.org/CorpusID:5030732, 1994.

Richardson, C. W., Foster, G. R., and Wright, D.: Estimation of Erosion Index from Daily Rainfall Amount, Transactions of the ASABE, 26, 153–0156, https://api.semanticscholar.org/CorpusID:108883838, 1983.

Rohlf, F. J.: Methods of comparing classifications, Annual Review of Ecology and Systematics, 5, 101–113, 1974.

Rosas, M. A. and Gutierrez, R. R.: Assessing soil erosion risk at national scale in developing countries: The technical challenges, a proposed methodology, and a case history, Science of the Total Environment, 703, 135 474, 2020.

Rutebuka, J., De Taeye, S., Kagabo, D., and Verdoodt, A.: Calibration and validation of rainfall erosivity estimators for application in Rwanda, Catena, 190, https://doi.org/10.1016/j.catena.2020.104538, cited by: 19, 2020.

Seager, R., Osborn, T. J., Kushnir, Y., Simpson, I. R., Nakamura, J., and Liu, H.: Climate variability and change of mediterranean-type climates, Journal of Climate, 32, 2887 – 2915, https://doi.org/10.1175/JCLI-D-18-0472.1, cited by: 207; All Open Access, Bronze Open Access, Green Open Access, 2019.

Shin, J.-Y., Kim, T., Heo, J.-H., and Lee, J.-H.: Spatial and temporal variations in rainfall erosivity and erosivity density in South Korea, CATENA, 176, 125–144, https://doi.org/https://doi.org/10.1016/j.catena.2019.01.005, 2019.

Silva, M. A. d., Silva, M. L. N., Owens, P. R., Curi, N., Oliveira, A. H., and Candido, B. M.: Predicting Runoff Risks by Digital Soil Mapping, Revista Brasileira de Ciência do Solo, 40, https://doi.org/10.1590/18069657rbcs20150353, 2016.

Sims, N. C., Newnham, G. J., England, J. R., Guerschman, J. P., Cox, S. J., Roxburgh, S. H., Viscarra Rossel, R. A., Fritz, S., and Wheeler, I.: Good Practice Guidance: SDG Indicator 15.3.1, Proportion of Land That Is Degraded Over Total Land Area, Version 2.0, Tech. rep., United Nations Convention to Combat Desertification (UNCCD), Bonn, Germany, 2021.

Song, Y., Yao, Y., Kong, W., Guo, L., Bao, K., Qiu, L., Shao, M., and Wei, X.: Effects of vegetation loss and soil erosion intensity on soil carbon dynamics across landscape position: Evidence from China's Loess Plateau, Agriculture, Ecosystems Environment, 396, 109 992, https://doi.org/https://doi.org/10.1016/j.agee.2025.109992, 2026.

Sun, L., Liu, F., Zhu, X., and Zhang, G.: High-resolution digital mapping of soil erodibility in China, Geoderma, 444, 116 853, https://doi.org/https://doi.org/10.1016/j.geoderma.2024.116853, 2024.

Tedla, H. Z., Taye, E. F., Walker, D. W., and Haile, A. T.: Evaluation of WRF model rainfall forecast using citizen science in a data-scarce urban catchment: Addis Ababa, Ethiopia, Journal of Hydrology: Regional Studies, 44, 101 273, https://doi.org/https://doi.org/10.1016/j.ejrh.2022.101273, 2022.

Todeschini, R., Ballabio, D., Termopoli, V., and Consonni, V.: Extended multivariate comparison of 68 cluster validity indices. A review, Chemometrics and Intelligent Laboratory Systems, p. 105117, https://doi.org/https://doi.org/10.1016/j.chemolab.2024.105117, 2024.

Tong, Y., Chen, Y., Qu, Y., Bento, V. A., Song, H., Qiu, H., Shui, W., Zeng, J., and Wang, Q.: Global rainfall erosivity: Observation, attribution, and projection, International Soil and Water Conservation Research, 14, https://doi.org/10.1016/j.iswcr.2025.12.005, cited by: 1; All Open Access, Gold Open Access, 2026.

Tu, A., Xie, S., Li, Y., Liu, Z., and Shen, F.: Effect of fixed time interval of rainfall data on calculation of rainfall erosivity in the humid area of south China, CATENA, 220, 106 714, https://doi.org/https://doi.org/10.1016/j.catena.2022.106714, 2023.

Vantas, K., Sidiropoulos, E., and Evangelides, C.: Rainfall Erosivity and Its Estimation: Conventional and Machine Learning Methods, in: Soil Erosion, edited by Hrissanthou, V. and Kaffas, K., chap. 2, IntechOpen, Rijeka, https://doi.org/10.5772/intechopen.85937, 2019.

Vantas, K., Sidiropoulos, E., and Loukas, A.: Estimating Current and Future Rainfall Erosivity in Greece Using Regional Climate Models and Spatial Quantile Regression Forests, Water, 12, https://doi.org/10.3390/w12030687, 2020.

Varón-Ramírez, V. M.: VimiVaron/Rainfall-Erosivity-Mexico: Rainfall- Erosivity-Mexico, https://doi.org/10.5281/zenodo.15468097, 2025.

Varón-Ramírez, V. M. and Guevara, M.: Advances in the study of soil erosion by water in Mexico published in Spanish, European Journal of Soil Science, 75, e13 458, https://doi.org/https://doi.org/10.1111/ejss.13458, 2024.

Varón-Ramírez, V. M., Gómez-Latorre, D. A., Arroyo-Cruz, C. E., Guevara Santamaría, M. A., and Prado Pano, B.: Daily Rainfall Series and Rainfall Erosivity in Mexico for Three Climatic Normals (1968–1997, 1978–2007, and 1988–2017), Version 3, https://doi.org/10.6073/pasta/dd2b30e28ee25ff2d60d8a9f436951d2, 2026.

Verstraeten, G., Poesen, J., Demarée, G., and Salles, C.: Long-term (105 years) variability in rain erosivity as derived from 10-min rainfall depth data for Ukkel (Brussels, Belgium): Implications for assessing soil erosion rates, Journal of Geophysical Research: Atmospheres, 111, https://doi.org/https://doi.org/10.1029/2006JD007169, 2006.

Wang, L., Li, Y., Gan, Y., Zhao, L., Qin, W., and Ding, L.: Rainfall erosivity index for monitoring global soil erosion, CATENA, 234, 107 593, https://doi.org/https://doi.org/10.1016/j.catena.2023.107593, 2024.

Wang, W., Yin, S., He, Z., Chen, D., Wang, H., and Klik, A.: Projections of rainfall erosivity in climate change scenarios for mainland China, CATENA, 232, 107 391, https://doi.org/https://doi.org/10.1016/j.catena.2023.107391, 2023a.

Wang, W., Yin, S., Yu, J., He, Z., and Xie, Y.: Long-term trends of precipitation and erosivity over Northeast China during 1961–2020, International Soil and Water Conservation Research, 11, 743–754, https://doi.org/https://doi.org/10.1016/j.iswcr.2023.04.002, advances in soil erosion research: processes, measurement, and modeling - A Special Issue in Honor of Dr. Mark Nearing, 2023b.

Wischmeier, W. H. and Smith, D. D.: Rainfall energy and its relationship to soil loss, Eos, Transactions American Geophysical Union, 39, 285–291, https://doi.org/https://doi.org/10.1029/TR039i002p00285, 1958.

Wischmeier, W. H. and Smith, D. D.: Predicting rainfall erosion losses : a guide to conservation planning, https://api.semanticscholar.org/CorpusID:129088976, 1978.

WMO: WMO Guidelines on the Calculation of Climate Normals, https://library.wmo.int/es/records/item/55797-wmo-guidelines-on-the-calculation-of-climate-normals, 2017.

WMO: Guidelines on Homogenization. WMO-No. 1245, https://library.wmo.int/idurl/4/57130, 2020.

WMO: Guide to Climatological Practices. WMO-No. 100, https://library.wmo.int/idurl/4/60113, 2023.

Xie, Y., qing Yin, S., yuan Liu, B., Nearing, M. A., and Zhao, Y.: Models for estimating daily rainfall erosivity in China, Journal of Hydrology, 535, 547–558, https://doi.org/https://doi.org/10.1016/j.jhydrol.2016.02.020, 2016.

Yan, Y., Wang, X., Hu, Z., Xu, X., Dai, Q., Mei, L., Gan, F., Jin, H., Wang, L., and Huang, C.: Exploring the spatiotemporal trends of extreme sub-hourly rainfall erosivity: Insights from karst plateaus in China, Journal of Hydrology: Regional Studies, 60, 102 590, https://doi.org/https://doi.org/10.1016/j.ejrh.2025.102590, 2025.

Yan, Z., Li, Z., and Xia, J.: Homogenization of climate series: The basis for assessing climate changes, Science China Earth Sciences, 57, 2891–2900, https://doi.org/10.1007/s11430-014-4945-x, 2014.

Yin, S., Xie, Y., Liu, B., and Nearing, M. A.: Rainfall erosivity estimation based on rainfall data collected over a range of temporal resolutions, Hydrology and Earth System Sciences, 19, 4113–4126, https://doi.org/10.5194/hess-19-4113-2015, 2015.

Yin, S., Nearing, M. A., Borrelli, P., and Xue, X.: Rainfall Erosivity: An Overview of Methodologies and Applications, Vadose Zone Journal, 16, vzj2017.06.0131, https://doi.org/https://doi.org/10.2136/vzj2017.06.0131, 2017.

Yozgatligil, C., Aslan, S., Iyigun, C., and Batmaz, I.: Comparison of missing value imputation methods in time series: the case of Turkish meteorological data, Theoretical and Applied Climatology, 112, 143–167, https://doi.org/10.1007/s00704-012-0723-x, 2013.

Yu, B. and Rosewell, C. J.: Rainfall erosivity estimation using daily rainfall amounts for South Australia, Soil Research, 34, 721–733, https://api.semanticscholar.org/CorpusID:128543482, 1996.

Zhang, Y.-G., Nearing, M., Zhang, X.-C., Xie, Y., and Wei, H.: Projected rainfall erosivity changes under climate change from multimodel and multiscenario projections in Northeast China, Journal of Hydrology, 384, 97–106, https://doi.org/https://doi.org/10.1016/j.jhydrol.2010.01.013, 2010.

Zhao, B., Zhang, L., Xia, Z., Xu, W., Xia, L., Liang, Y., and Xia, D.: Effects of Rainfall Intensity and Vegetation Cover on Erosion Characteristics of a Soil Containing Rock Fragments Slope, Advances in Civil Engineering, 2019, 7043 428, https://doi.org/https://doi.org/10.1155/2019/7043428, 2019.